THE ROLE OF THROMBOXANE A_2 RECEPTORS IN PODOCYTES IN DIABETIC KIDNEY DISEASE

Roya Shaji

Thesis submitted to the Department of Cellular and Molecular Medicine in partial fulfillment of the requirements for the degree of Master of Science

Faculty of Medicine
University of Ottawa
Ottawa, Ontario, Canada

ABSTRACT

Thromboxane receptor (TPr) activity is elevated in diabetes and contributes to complications of diabetic kidney disease (DKD). TPr blockade appears to have therapeutic potential. Several rodent models of DKD show attenuation of renal damage and proteinuria upon administration of the TPr antagonist, S18886. However, the cellular targets that underlie the injurious effects of TPr activation in DKD remain to be elucidated.

A pilot study in our laboratory subjected a conditionally-immortalized mouse podocyte cell line to high glucose (25 mM D-glucose) and equibiaxial mechanical stretch (an *in vitro* simulator of increased glomerular capillary pressure associated with glomerular hyperfiltration in early diabetes). qRT-PCR revealed that exposure of podocytes to mechanical stretch (10% elongation) and high glucose for 6 hours yielded a 9-fold increase in TPr mRNA levels vs. controls (non-stretch, 5mM D-glucose + 25mM L-glucose) ($p<0.05$, $n=5$). We hypothesized that TPr expression and activity are increased in podocytes during the onset of DKD resulting in maladaptive effects on this key glomerular filtration barrier cell type.

We showed that enhanced TPr signaling threatens podocytes viablility. Cultured podocytes treated with the TPr agonist, U-46619 (1 μM) for 24 hours are more vulnerable to apoptosis as quantified by Hoescht 33342 (20% cell death $p<0.001$, $n=3$) , TUNEL (30-fold increase, ns, $n=3$) and Annexin-V labeling (3-fold increase, $p <0.001$, $n=3$).

To further support these *in vitro* findings, we developed a transgenic mouse with podocyte-specific overexpression of TPr. A construct consisting of a desensitization resistant mutant of the human TPr with both N- and C-terminal HA-epitope tags under the control of an 8.3 kb fragment of the immediate 5' mouse *NPHS1* promoter was cloned, isolated and injected into FVB/n oocytes that were implanted into pseudopregnant CD1 females. Founders were characterized for TPr transgene expression, and TPr transgene mRNA levels were detected by qRT-PCR.

Our *in vitro* results suggest that increased TPr expression in podocytes of diabetic mice may contribute to filtration barrier damage and have important implications in the development and progression of DKD.

Acknowledgements

These past two years have taught me immensely about myself as a scientist and as a person. Completion of this endeavour is largely a testament to my resilience. I can humbly say that I have come out of this experience stronger, smarter and with superior reflexes.

I could not have succeeded without the guidance and encouragement of my supervisor, Dr Chris Kennedy. I must also express profound thanks to my advisory committee members, Dr Tonye and Dr Turksen, for helping me to realize the full potential of my project. In mastering the art of troubleshooting, I am grateful for the expert teachings of Alexei Gutsol, Dylan Burger, Kaede Takami, Jean-François Thibodeau and Erin Stitt-Cavanagh.

I owe an interminable debt to K.B., whose support and good humour have saved me on more than one occasion.

To my family and especially Nohad, my mother, friend and everlasting cheerleader.

Thank you.

DECLARATION

I certify that this thesis does not incorporate without acknowledgement any material previously submitted for a degree in any university. To the best of my knowledge, this thesis does not contain material previously written by another except where due reference is made in the text.

I authorize the University of Ottawa to reproduce this thesis in whole or in part at the request of another institution for the purpose of academic research.

Roya Shaji

TABLE OF CONTENTS

FIGURES

ABBREVIATIONS

2-HE	2-hydroxyethidium
12-HETE	12- hydroxyeicosatatraenoic acid
12-LOX	12- lipoxygenase
ACR	albumin-to-creatinine ratio
AT_1	angiotensin II receptor type 1
ANOVA	analysis of variance
bp	base pair
BSA	bovine serum albumin
CD2AP	CD2-associated protein
Ca	calcium
cAMP	cyclic adenosine monophosphate
cDNA	complementary DNA
COX	cyclooxygenase
DAG	diacylglyercol
DHE	dihydroethidium
DKD	diabetic kidney disease
DTPA	Diethylene triamine pentaacetic acid
EIA	enzyme immunoassay
EP_1	prostaglandin E receptor 1
EP_4	prostaglandin E receptor 4
ESRD	end-stage renal disease
FITC	fluorescein isothiocyanate

FBS	fetal bovine serum
FSH	follicle-stimulating hormone
GAPDH	glyceraldehyde-3-phosphate dehydrogenase
GBM	glomerular basement membrane
GFB	glomerular filtration barrier
GFR	glomerular filtration rate
G_i	inhibitory G
GPCR	G protein-coupled receptor
G_s	stimulatory G
GTPase	guanosine triphosphatase
GTX	glutathione peroxidase
HBSS	Hank's balanced salt solution
hCG	human chorionic gonadrotropin
HPLC	high-performance liquid chromatography
IF	immunofluorescence
IL-6	interleukin-6
INF-γ	interferon gamma
IP_3	inositol-1,4,5-trisphosphate
kB	kilobase
LB	Luria Bertani
LH	luteinizing hormone
mRNA	messenger ribonucleic acid
NADPH	nicotinamide adenine dinucleotide phosphate
NO	nitric oxide

NOD	non-obese diabetic
NPHS1	nephrin
ns	not significant
PAN	puromycin aminocleoside
PBS	phosphate buffered saline
PCR	polymerase chain reaction
PFA	paraformaldehyde
PKC	protein kinase C
PI	propidium iodide
PIP_2	phosphatidylinositol 4,5-bisphosphate
P_{gc}	glomerular capillary pressure
PGD_2	prostaglandin D_2
PGE_2	prostaglandin E_2
PGF_2	prostaglandin F_2
PGH_2	prostaglandin H_2
PGI_2	prostacyclin
PI	phosphatidylinositol
PLC	phospholipase C
PMSG	pregnant mare’s serum gonadotropin
PTEC	proximal tubular epithelial cell
qRT-PCR	quantitative reverse-transcription polymerase chain reaction
RhoGEF	Rho guanine nucleotide exchange factor
RIPA	Radioimmunoprecipitation assay

RNA	ribonucleic acid
ROCK	Rho-associated protein kinase
ROS	reactive oxygen species
rpm	rotations per minute
rpm	rotations per minute
SDS	sodium dodecyl sulfate
SEM	standard error mean
SOC	super optimal broth with catabolite repression
STZ	streptozotocin
TG	transgenic
TPr	thromboxane A_2 receptor
TPr^{mut}	mutant thromboxane A_2 receptor
TxA_2	thromboxane A_2
TxB_2	thromboxane B_2
TXS	thromboxane synthase
TUNEL	terminal deoxynucleotidyl transferase dUTP nick end labeling
UV	ultraviolet
WT	wildtype

1. INTRODUCTION

1.1. THE KIDNEY AND ALBUMINURIA

As blood flows through the kidneys, it is filtered by roughly two million glomeruli, each containing a multi-layered barrier that selects molecules based on size and charge. When filtration capability is undermined, a condition known as albuminuria can occur, where vital plasma proteins including albumin leak through and pass into the urine. Loss of serum albumins, which constitute 60% of human plasma protein, is particularly injurious because they regulate blood volume by preserving oncotic pressure.

Albuminuria is currently the best available non-invasive method for early detection of kidney disease in diabetic patients who account for a 40% of cases of end-stage renal disease (ESRD) in North America due to diabetic kidney disease (DKD)[1]. DKD is a form of chronic kidney disease occurring in patients with either type I or type II diabetes.

1.2. DIABETIC KIDNEY DISEASE

DKD is defined by three stages: microalbuminuria, proteinuria with reduced glomerular filtration rate (GFR) and ESRD[2].

I. Microalbuminuria (Incipient Nephropathy)

The onset of DKD in diabetic patients is characterized by microalbuminuria, or an increased urinary albumin excretion of 30 to 200 mg over 24 hours. It is accompanied by increased GFR, or hyperfiltration, which describes an increased flow rate of filtered fluid through the kidney.

II. Clinical Nephropathy: Proteinuria and decreasing GFR

Following some years of microalbuminuria, GFR declines below normal and proteinuria is detectable. Proteinuria is defined as albumin excretion exceeding 200 mg/day and is universal marker of DKD. In patients who develop DKD, proteinuria increases with time leading to nephrotic syndrome exceeding 3 g/day. Hypertension is present in the majority of patients at this stage.

III. End-stage renal disease

The complete or near-complete failure of the kidneys renders them unable to remove wastes or concentrate urine. Renal replacement therapy, either dialysis or transplantation, is necessary to maintain life.

1.3. GLOMERULAR FILTRATION BARRIER

As molecules in the plasma pass through the lumen of glomerular capillary loops, they are subject to a three-layered filtration unit: an endothelial cell layer, a glomerular basement membrane (GBM) and finally, the podocyte cell layer (Fig. 1.1). The endothelial layer prevents the passage of cells, while the GBM, with its negatively charged glycoproteins, blocks large plasma proteins from entering the urine. Podocytes also possess negatively charged membrane domains that effectively limit the passage of molecules such as albumin, however the slit-diaphragm is believed to play the most selective role in molecular passage.

Although research has shown that all layers of the barrier are crucial for proper function, over recent years, the podocyte has become highlighted as a pivotal player, making it an important potential therapeutic target. This is particularly true when recognizing that 90% of ESRD cases share the common theme of podocyte injury in glomerular filtration dysfunction.

Figure 1.1. Glomerular filtration barrier. Molecules in the plasma encounter a three-layered filtration unit: an endothelial cell layer, GBM and podocyte cell layer. Nephrin, podocin and CD2AP are just a few pivotal members of an extensive network of structural and signaling proteins that interact to maintain a permeable yet size-selective slit diaphragm that serve to bridge podocyte foot processes (pedicels)

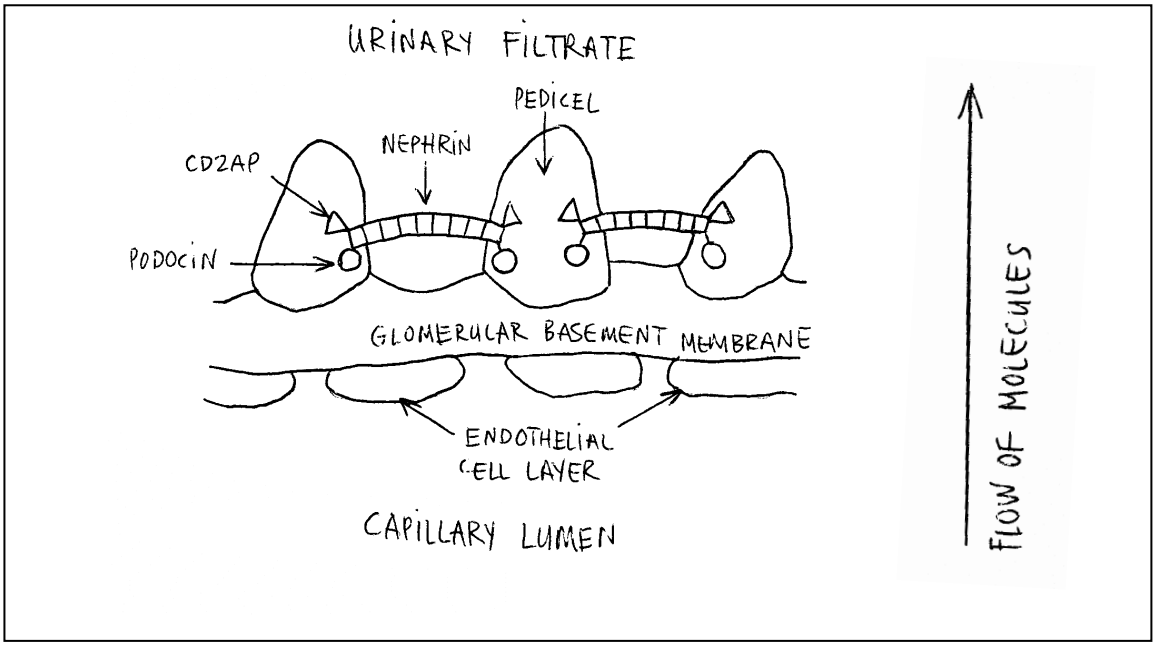
URINARY FILTRATE
PEDICEL
NEPHRIN
CD2AP
PODOCIN
GLOMERULAR BASEMENT MEMBRANE
ENDOTHELIAL CELL LAYER
CAPILLARY LUMEN
FLOW OF MOLECULES

1.4. PODOCYTE ARCHITECTURE

Podocytes are highly specialized and terminally differentiated epithelial cells that form inter-digitating foot processes with their neighbours to form filtration slits (Fig. 1.2). A network of pivotal structural and signaling proteins bridges these slits, including nephrin, podocin and CD2-associated protein (CD2AP) that interact to maintain a permeable yet size-selective slit diaphragm (Fig. 1.1). The podocytes and their connecting slit diaphragms act as a crucial filtering sieve and possess both size and charge-selective qualities[3].

In the disease state, podocytes may alter their morphology (ie. foot process widening/ effacement, cytoskeletal abnormalities), detach from the filtration barrier or die[4]. These changes inherently compromise the integrity of the barrier (Fig. 1.3). proximal tubule epithelilal cells (PTEC). PTECs make up the proximal convoluted tubule, a portion of the nephron which leads from the Bowman's capsule to the loop of Henle and is involved in the reuptake of physiologically filtered albumin reabsorption. The failure of the proximal convoluted tubule to take up albumin also diminishes nephron function and contribute to albuminuria observed in patients with DKD[4].

Histologically, DKD features the enlargement of the kidneys, hypertrophy of tubular cells and the glomerulus, mesangial expansion, thickening of the GBM due to enhanced collagen deposition, vascular lesions in the glomerular vasculature and the appearance of extracellular matrix protein-containing Kimmelstiel-Wilson nodules (Fig. 1.4).

1.5. DKD AND THE PODOCYTE

Studies looking at kidney biopsies from patients with type I and II diabetes noted a decline in podocyte number that could predict subsequent proteinuria[5-7]. Indeed, podocyte damage and loss is now regards as one of the key initial events in glomerular injury and recognized as the most direct cause of proteinuria, occurring early in DKD and predicting the pace of disease progression[8-9,10]. As treatment for kidney disease begins to shift from detection and treatment to prevention and prediction, investigating the causes of early injury to the podocyte can help conceive the therapies needed to protect them.

Figure 1.2. Podocytes. Podocytes wrap around the capillaries of the glomerulus. Long processes extend from the cell body and interdigitate with neighbouring podocytes, leaving slits between them. Plasma is filtered through slit diaphragms which bridge these slits.

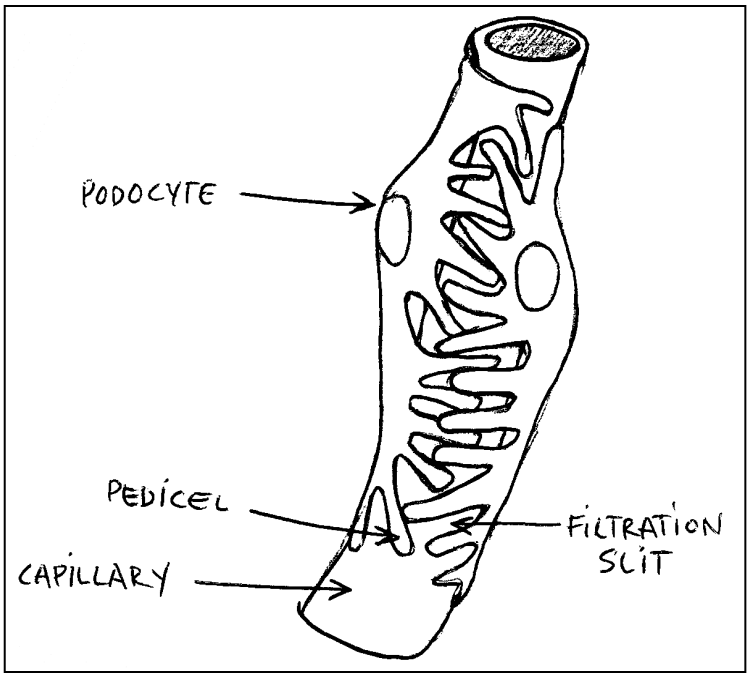
PODOCYTE
PEDICEL
CAPILLARY
FILTRATION SLIT

Figure 1.3. Podocyte defects. In DKD, downregulation and/or relocalization of invaluable proteins like nephrin destroy the integrity of the slit diaphragm. Podocytes can undergo drastic morphological changes that result in self-effacing loss of pedicels. Podocytes may also detach from the glomerular filtration barrier which can be caused by cytoskeletal abnormalities but also by dysfunctional basal integrins which normally anchor podocytes into the glomerular basement membrane. Podocytes may directly undergo apoptosis, resulting in reduced cell numbers in the glomerulus. This effectively creates holes in the filtration barrier which permit the free flow of proteins into the primary urine of Bowman's space.

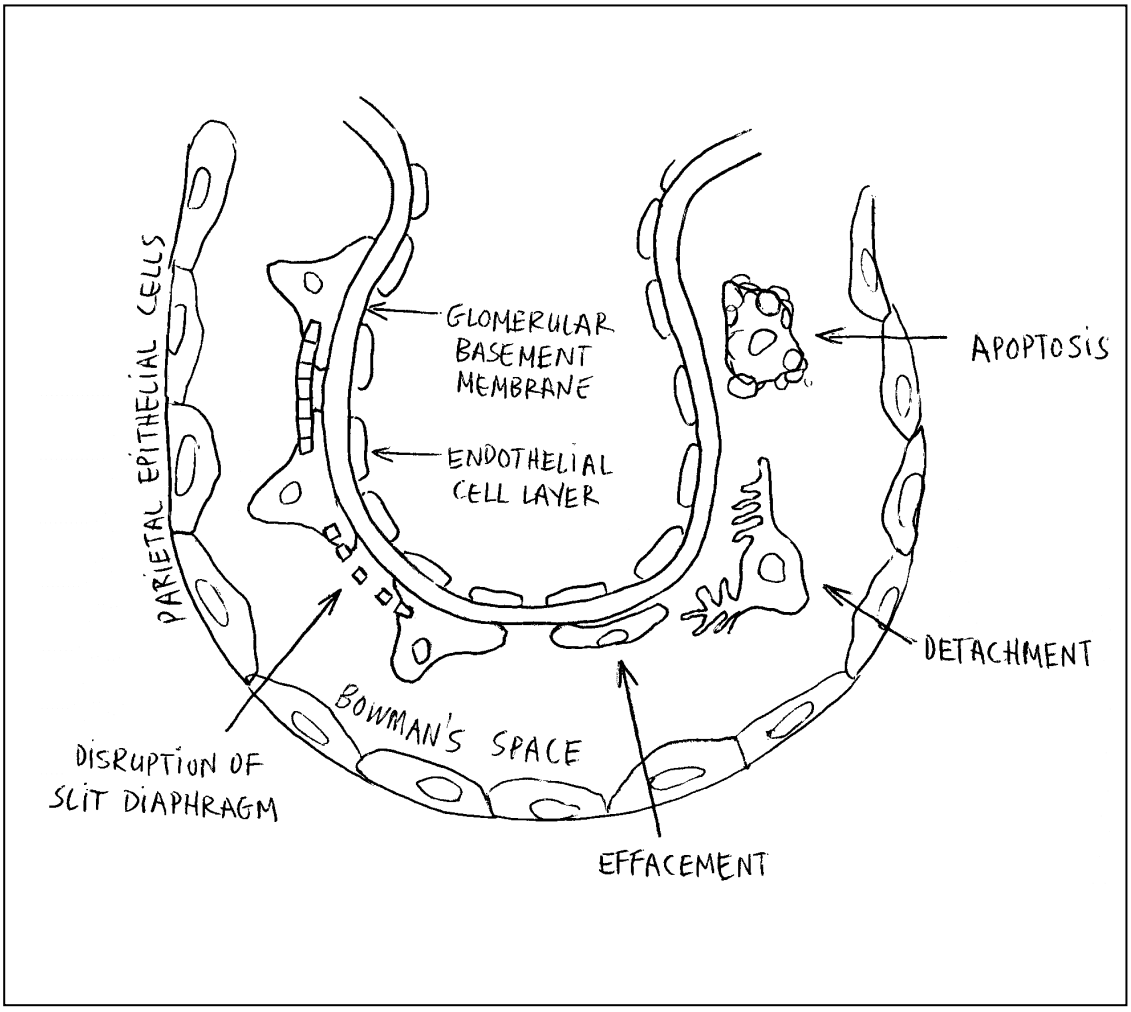
PARIETAL EPITHELIAL CELLS
GLOMERULAR BASEMENT MEMBRANE
ENDOTHELIAL CELL LAYER
APOPTOSIS
DETACHMENT
BOWMAN'S SPACE
DISRUPTION OF SLIT DIAPHRAGM
EFFACEMENT

Figure 1.4. Glomerular changes in DKD. (A) Healthy glomerulus. (B) Diabetic glomerulus with typical GBM thickening, mesangial cell hypertrophy and expansion which reduces filtration surface and capacity, leading to subsequent podocyte injury and loss. (C) Light micrograph showing architectural disruption of mesangial cells and Kimmelstiel-Wilson nodule (Taken from JA Jefferson et al. 2008. Pathology images courtesy of Jolanta Lowalewksa)

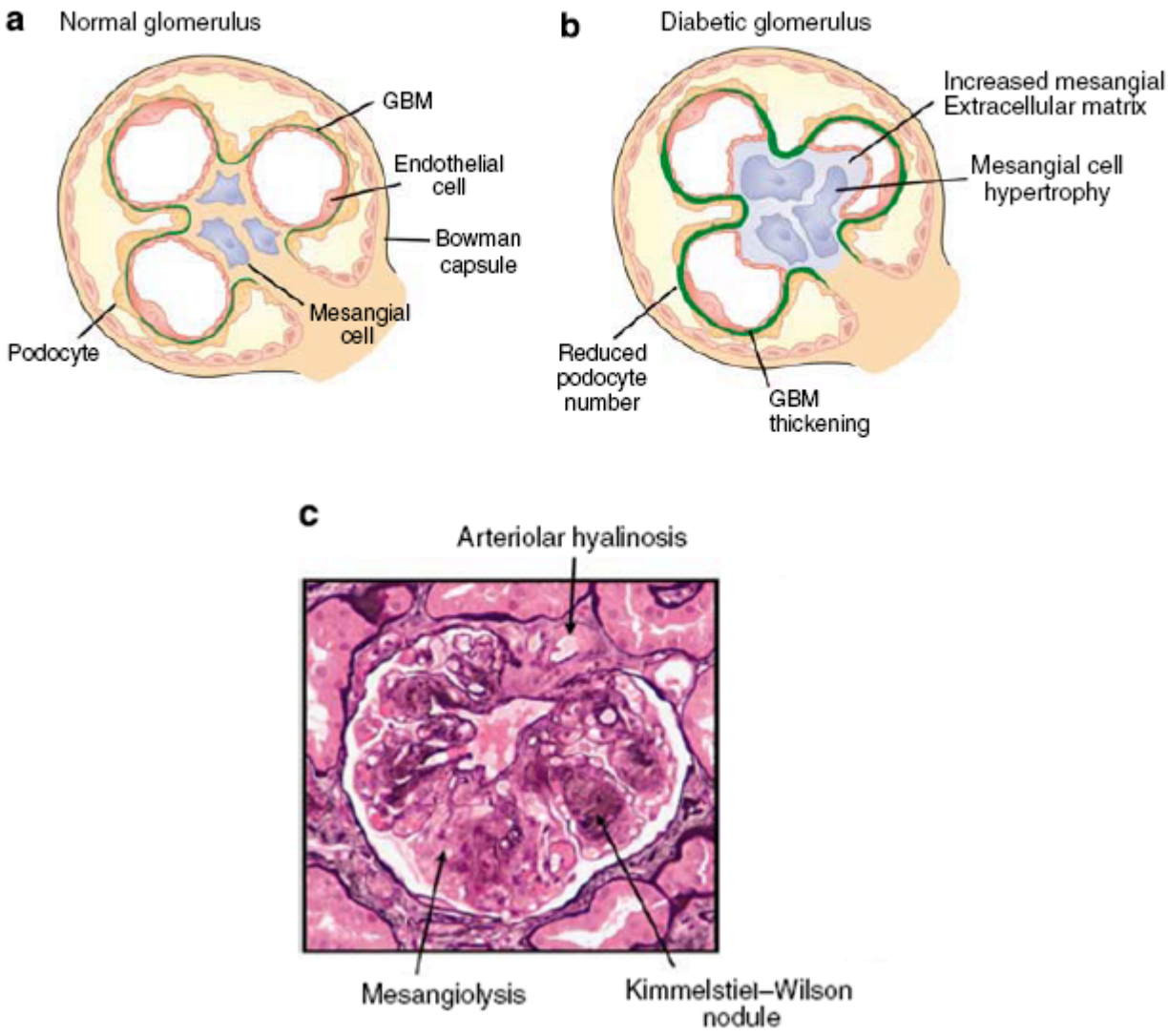

JA Jefferson et al. 2008

1.6. EFFECTORS OF PODOCYTE INJURY

1.6.1. Hyperglycemia and hypertension

Together, hyperglycemia, angiotensin II and increased glomerular capillary pressure (P_{gc}) activate injurious signal transduction pathways in the podocyte. Podocyte dysfunction and apoptosis are linked to glucose-induced reactive oxygen species (ROS) production[10,11]. Glucose can also alter slit diaphragm and actin cytoskeleton properties. Indirectly, podocyte injury leads to reduced insulin responsiveness and glucose uptake. Diminished glucose uptake is hypothesized to inhibit the structural remodeling capability of podocytes in response to the enhanced mechanical forces exerted within the glomerulus that are associated with increased blood flow[12].

Increased blood flow in the kidney is induced by the renin-angiotensin-aldosterone system (RAAS), responsible for maintaining blood pressure as well as fluid and electrolyte balance. An activated RAAS is a major cause of target organ damage due to hypertension. The main effector in the system, angiotensin II, causes vasoconstriction by altering the resistance of the afferent and efferent arterioles of the glomerulus and contributes to increased glomerular capillary pressure (P_{gc})[2]. Angiotensin II has also been shown to mediate nephrin suppression. Furthermore, podocytes possess a local angiotensin II system which can be activated by high glucose, proteinuria and increased P_{gc}[13].

Current therapeutic approaches are focused on hyperglycemic and blood pressure control. Although early administration of these therapies can slow disease progression, they can neither stop nor reverse damage once DKD has already clinically manifested, implicating other effectors in podocyte dysregulation.

1.6.2. Cyclooxygenase and prostanoids

Recent studies implicate the enzyme cyclooxygenase (COX) in podocyte injury. Several rodent models of kidney disease confirm COX induction in podocytes[9,14-16]. Mechanical strain as a mimic of increased P_{gc} has been shown to induce COX-2 expression in cultured mouse podocytes, causing injury[17]. COX inhibitors can slow the progression of glomerular injury and reduce proteinuria[14-16,18,19]. The beneficial effects of these inhibitors are undermined by their adverse effects on the cardiovascular system and their reduction of GFR and renal blood flow [20,21]. This is because COX synthesizes five prostanoids that bind to their respective receptors to elicit unique and widespread roles in the maintenance of renal homeostasis and function as well as other systems.

COX has two isoforms, COX-1 and COX-2. Both play constitutive housekeeping roles in the body; however the latter is induced by inflammatory mediators and mitogens, playing a key role in pathophysiological processes[22]. Prostanoids derived from COX-2 are important mediators of vascular tone as well as salt and water balance[23]; they are rapidly degraded and act in paracrine or autocrine fashion via their specific G protein-coupled receptors (GPCRs) to provoke distinct G

protein-coupled signaling pathways. Molecules synthesized via the COX pathway are prostacyclin PGI_2 and prostaglandins PGF_2, PGE_2 and PGD_2 (Fig. 1.5).

1.7. TXA_2 AND THE TP RECEPTOR

Thromboxane A_2 (TxA_2) is synthesized through the combined actions of COX and thromboxane synthase (TXS). TxA_2 is synthesized in a two-step process involving the conversion of an essential fatty acid found in the phospholipid bilayer, arachidonic acid, into prostaglandin H_2, by COX, followed by the conversion of prostaglandin H_2 to thromboxane A_2 by TXS[24]. TxA_2 is a potent vasoconstrictor; its activation can reduce renal plasma flow and glomerular filtration rate, and contract glomeruli and mesangial cells[25,26].

Thromboxane A_2 receptor (TPr) binds TxA_2 and additional arachidonic acid metabolites, including 12- hydroxyeicosatatraenoic acid (12-HETE) and isoprostanes, all of which act as agonists of TPr. 12-HETE is produced by the oxidoreductase enzyme, 12 LOX (12- lipoxygenase); both of these products are elevated in diabetes and implicated in DKD pathogenesis[27-29]. Isoprostanes are formed from the peroxidation of arachidonic acid catalyzed by free radicals. Isoprostane levels are also increased in diabetes[30].

In the rat kidney, TPr localizes in glomeruli and renal tubules. In the glomerulus, it is distributed in podocytes, mesangial cells and parietal epithelial cells of the Bowman's capsule[31]. Depending on the cell type, TPr signals via several G-proteins to regulate numerous physiological actions. TPr couples to $G_{12/13}$ to promote

activity of the small GTPase protein RhoA through RhoGEF (guanine nucleotide exchange factor) resulting in modulation of both the cytoskeleton and cell survival. TPr also promotes G_s and G_i stimulation to modulate cAMP levels[32]. TPr also couples to G_q to elicit phospholipase C (PLC)-mediated phosphatidylinositol (PI) hydrolysis and intracellular calcium mobilization in platelets and vascular smooth muscle cells triggering aggregation and vasoconstriction, respectively[33-35]. The major G proteins which communicate with TPr are G_q and G_{13}[24] (Fig. 1.5).

Figure 1.5. Prostanoid synthesis and TPr signal transduction pathways. Membrane phospholipids are converted to arachidonic acid via phospholipase A_2 or phospholipase C. Arachidonic acid can be converted into a variety of products depending on the enzyme. COX-1 and COX-2 convert arachidonic acid into prostaglandin H_2 which may then convert to several different types of prostanoids depending on the synthase. The actions of TXS convert PGH_2 to TxA_2 . Isoprostanes are formed from the peroxidation of arachidonic acid by free radicals. Finally 12-LOX can convert arachidonic acid into 12-HETE. TxA_2, isoprostanes and 12-HETE are all TPr agonists that activate G-signaling cascades. TPr couples to $G_{12/13}$ to promote activity of the small GTPase protein RhoA through RhoGEF modulating cytoskeleton and cell survival. TPr can promote G_s and G_i stimulation to modulate cAMP levels. TPr also couples to G_q to elicit PLC-mediated PI hydrolysis and intracellular calcium mobilization in platelets and vascular smooth muscle cells to trigger aggregation and vasoconstriction, respectively.

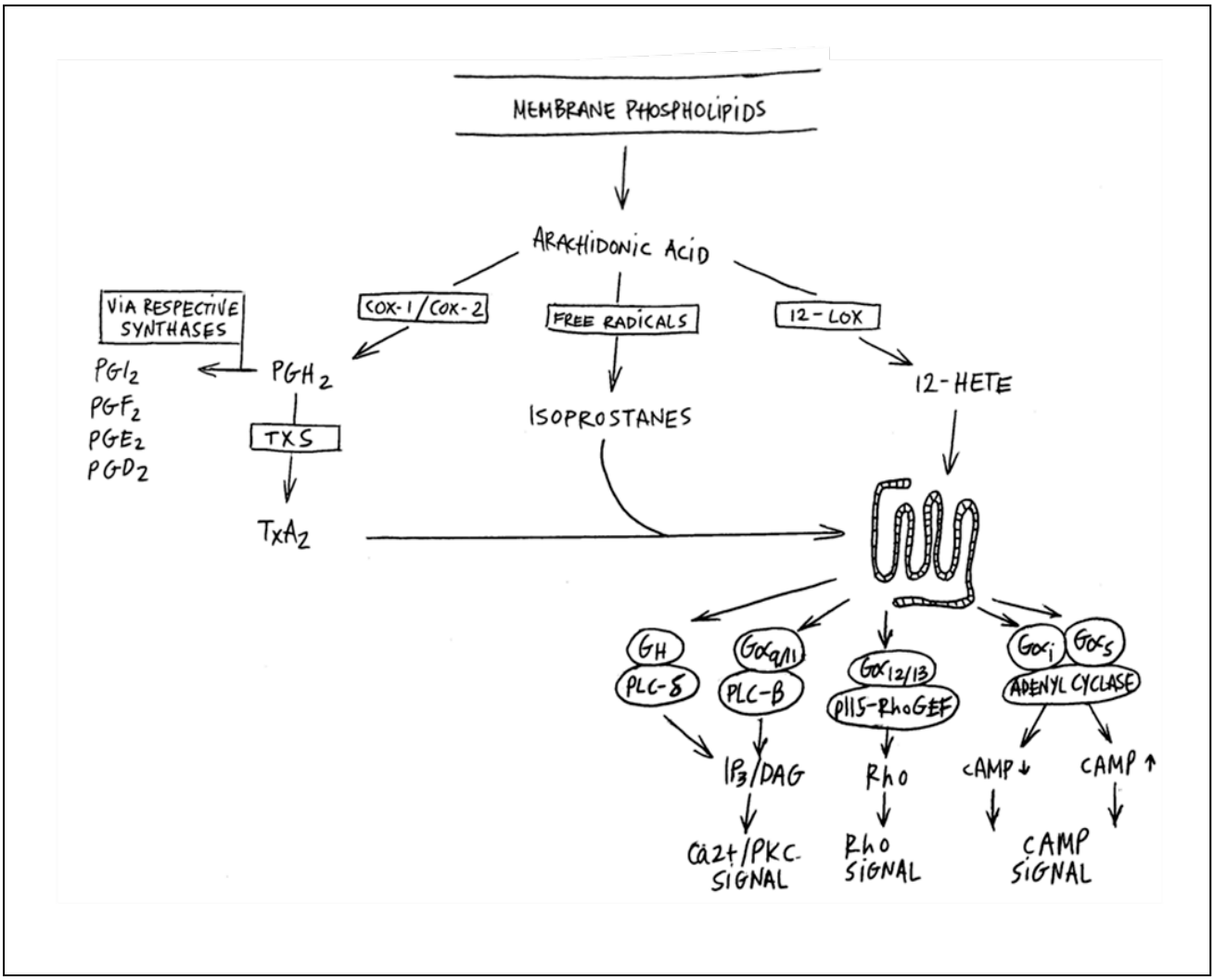
MEMBRANE PHOSPHOLIPIDS
ARACHIDONIC ACID
VIA RESPECTIVE SYNTHASES
COX-1 / COX-2
FREE RADICALS
12-LOX
PGI2
PGF2
PGE2
PGD2
PGH2
TXS
TxA2
ISOPROSTANES
12-HETE
GH
PLC-δ
Gαq/11
PLC-β
G12/13
p115-RhoGEF
Gαi
GαS
ADENYL CYCLASE
IP3/DAG
Rho
cAMP ↓
cAMP ↑
Ca2+/PKC SIGNAL
Rho SIGNAL
cAMP SIGNAL

2. RATIONALE

TPr inhibition is protective in several mouse models of DKD[30,36]. Xu and colleagues found that pharmacological TPr blockade attenuates oxidant stress, inflammation, microalbuminuria, and histological evidence of DKD in a mouse model of type II diabetes, implying a clear role for the TPr in filtration barrier dysfunction[30]. Whether podocytes are cellular targets for these deleterious actions has not been investigated. Dissecting the roles of this COX-2 derivative in glomerular function may facilitate development of more focused therapeutic approaches minus the adverse effects caused by COX-2 inhibitors.

Studies by Melina Marin-Leblanc in our laboratory have shown that TPr expression in cultured podocytes is significantly enhanced in response to conditions that mimic those encountered during diabetes - high glucose and mechanical stretch (Fig. 1.6).

Figure 1.6. TPr mRNA expression in cultured podocytes under high glucose and mechanical stretch. Results are presented as mean ± SEM ($p<0.05$, $n=5$) and are expressed as fold increase of control. 'High glucose +stretch' mRNA levels were 9 times higher compared to controls at 6 hours. mRNA was assayed by qRT-PCR and normalized against GAPDH. Control group received 5mM D-glucose + 20 mM L-glucose (normal glucose) and no stretch, remaining groups received either 25mM D-glucose (high glucose) or equibiaxial mechanical stretch (stretch) or a combination of both (high glucose + stretch). mRNA levels were measured at 2 (light grey columns), 4 (grey columns) and 6 hours (black columns).

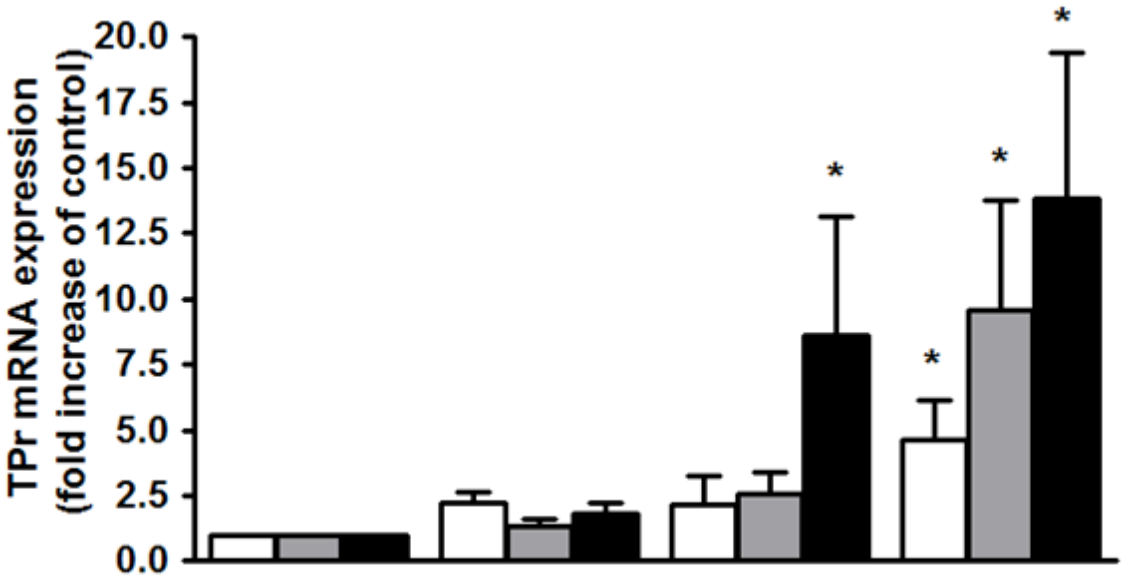

normal glucose	+	+	-	-
stretch	-	+	-	+
high glucose	-	-	+	+

3. HYPOTHESIS

In diabetic nephropathy, thromboxane A2 receptor activity is responsible for podocyte loss via apoptosis.

4. OBJECTIVES

I. Develop a podocyte-specific desensitization-resistant TPr genetic construct

II. Generate and characterize transgenic mice

III. Study effects of TPr activation on cultured mouse podocytes

5. MATERIALS AND METHODS

5.1. MOLECULAR CLONING STRATEGY

5.1.1. Plasmid

I. Mammalian expression vector pcDNA3

Both TPr gene and nephrin (NPHS1) promoter were originally cloned into separate plasmids of mammalian expression vector pcDNA3 (Invitrogen) .This plasmid contains an ampicillin-resistance gene, allowing for selection of our future recombinant clones by growing them on ampicillin-containing medium (Fig. 5.1).

II. TPr gene

Dr Spurney and colleagues previously cloned the mouse TPr gene with both N and C terminal hemagglutannin tags into the EcoR1/Apa1 sites of pcDNA3 5.7 kB in length. The TPr gene was mutated at position 321 (proline→glycine), 322 (arginine→alanine), 328 (arginine→alanine) and the first N-linked glycosylation site mutated to isoleucine. These mutations confer the receptor with a delayed onset of agonist-induced desensitization. Alteration at these sites prevent G protein-coupled receptor kinases from phosphorylating them in order to signal their removal from the cell membrane.

III. NPHS1 promoter gene

We took advantage of a plasmid previously developed in our laboratory, a mutant EP_4 transgene linked to the NPHS1 promoter (8.3 kB). Of particular interest for this project was isolation of the NPSH1 promoter located between HindIII/XhoI sites in pcDNA3.

Figure 5.1. Mammalian plasmid pcDNA 3. Plasmid segments are not to scale. Some highlighted features include the gene conferring ampicillin resistance to *E. coli* that take up the plasmid. Incubating *E.coli* on ampicillin-coated agar plates selects for these colonies. The *BamHI* and *RsrII* sites were the sites chosen for cutting and ligating the vector and insert to form our transgenic construct. A primer specific for the SP6 promoter of pcDNA3 was later used for construct sequencing purposes.

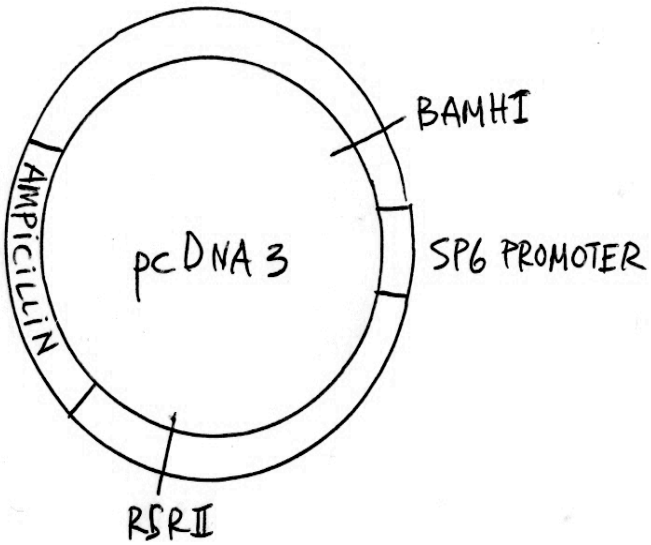
BAMHI
SP6 PROMOTER
pcDNA 3
AMPICILLIN
RSRII

5.1.2. *NPHS1-2xHA-TPr^{mut}* construct

An 8.3-kb fragment of the mouse *NPHS1* promoter was cloned immediately upstream of the *2XHA-TPr^{mut}* sequence, in order to drive podocyte-specific expression of *TPr^{mut}* (Fig. 5.2).

5.1.3. Selecting clones of interest I

TPr^{mut} and *NPHS1* were propagated in *E.coli* Subcloning Efficiency DH5α cells (Invitrogen). The following steps were performed for each both genes.

I. Cell transformation

Cells were thawed on wet ice and 1µl of plasmid was added to 100 µl of cells into chilled polypropylene Falcon 2059 tubes. Tubes were mixed by gentle tapping and left on ice for 30 minutes. Cells were heat-shocked for 45 seconds in a 42°C water bath. Cells were placed back on ice for 2 minutes. Room temperature super optimal broth with catabolite repression (SOC) medium (1 ml) was added. Tubes were placed in an orbital shaker. Samples of 100 µl, 150 µl, 200 µl of reaction containing plasmid DNA was transferred to pre-poured agar plates containing ampicillin (100 µg/ml) using the spread plate technique. Plates were incubated inverted at 37°C overnight to allow colonies to form.

II. Amplifying colonies

The following day, single colonies were picked with a sterile toothpick and placed in respective tubes containing 3 ml of Luria Bertani broth (LB) and 3 µl of ampicillin. Tubes were placed in a shaker at 37°C in an orbital shaker at 225 rpm for 5 to 6 hours. The tube containing the least translucent broth (broth opacity acting as an indicator of cell growth) was transferred to a baffle flask containing 150 ml LB and 150 µl ampicillin and grown overnight at 37°C, in an orbital shaker at 240 rpm.

III. Harvesting the culture

Flask was split into 3 tubes and centrifuged for 15 minutes at 3000 rpm, 10°C. The supernatant liquid broth was poured off and pelleted cells were stored at -80°C as frozen stocks.

IV. Isolating the plasmids

Each cell culture was subjected to an alkaline-SDS lysis procedure using the GenElute Plasmid Miniprep Procedure (Sigma-Aldrich) according to manufacturer's instructions.

Figure 5.2. Molecular cloning strategy for *NPHS1-2xHA-TPr^{mut}* construct. Plasmid segments are not to scale. Vector (plasmid containing *NPHS1* promoter) and insert (plasmid containing *2xHA-TPr^{mut}*) were cut with respective enzymes, *XhoI* and *BamHI*, blunted, then cut again with *RsrII.* Ligation of segments in a blunt-blunt, stick-sticky fashion allowed insert placement downstream of vector, conferring podocyte-specific expression of *TPr^{mut}* driven by the *NPHS1* promoter.

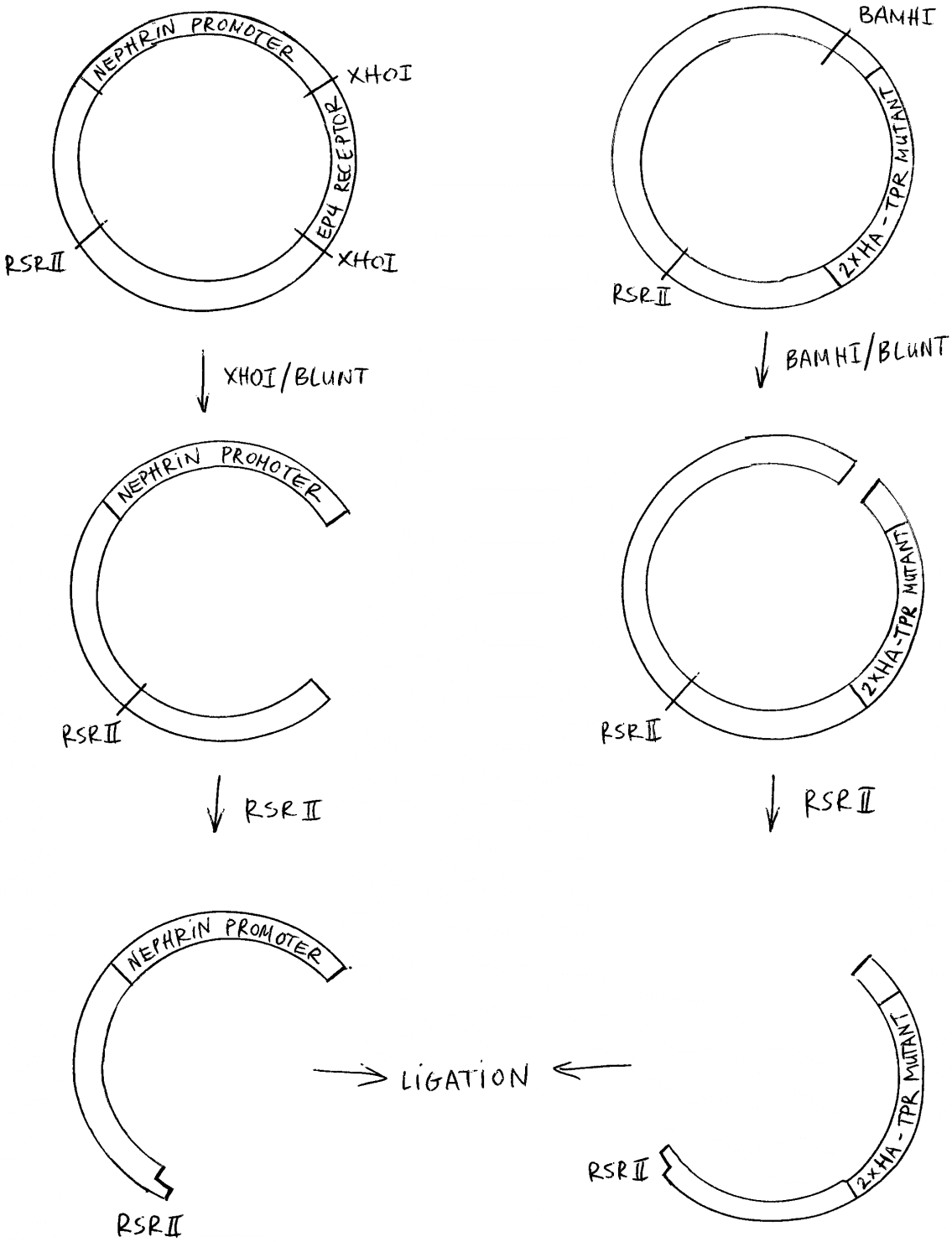
NEPHRIN PROMOTER
XHOI
EPH RECEPTOR
XHOI
RSRII
XHOI/BLUNT
NEPHRIN PROHOTER
RSRII
RSRII
BAMHI
2XHA-TPR MUTANT
RSRII
BAMHI/BLUNT
2XHA-TPR MUTANT
RSRII
RSRII
NEPHRIN PROMOTER
RSRII
LIGATION
2XHA-TPR MUTANT
RSRII

5.1.4. Restriction/ligation cloning

Restriction enzymes and T4 DNA polymerase were used to create two compatible DNA fragments suitable for ligation. To do this, a blunt end and a sticky end (*RsrII* site) were first molded on the TPr gene-containing plasmid. The ends of *NPHS1* promoter were then molded similarly to facilitate ligation via blunt-blunt adhesion and sticky-sticky adhesion based on complementary nucleotide pairing. The first cloning step required molding a sticky and blunt end on the plasmid containing the TPr gene:

I. Sticky end formation

Sticky ends were created by cutting the plasmid with *BamH1*. A reaction mixture of 30 µl containing plasmid (1µg), NEB Buffer 2 (1x), BSA (1x), ddH_20 and *BamH1* (1:15) was incubated at 37°C for 4 hours.

II. Blunt end formation

Sticky ends were blunted by heat inactivating the reaction at 65°C for 20 minutes, and then adding it to a T4 DNA polymerase reaction mixture containing T4 DNA polymerase buffer, 82.5 µM dNTP mix, T4 DNA polymerase (10 U) and water (Invitrogen). The reaction was incubated at 12°C for 20 minutes.

III. Purification

DNA fragments were purified and concentrated from restriction enzymes, buffer salts, polymerases and dNTPs using the QIAEXII Protocol for Desalting and Concentrating DNA Solutions (Qiagen).

IV. Sticky end formation at RsrII site

A sticky end was created at the *RsrII* site by incubating a reaction mixture containing the plasmid (40 µl eluate), NEB Buffer 4, BSA (1x) and *RsrII* at 37°C for 4 hours.

V. Isolation

The reaction mixture was mixed with loading buffer and loaded onto a 1.5% agarose gel. Gel electrophoresis revealed three segments of digested DNA: single-cut plasmid, a 4.2 kB drop-out containing the TPr gene and a 3.5 kB drop-out containing the remainder of the pcDNA backbone. A long wave UV lamp (365 nm) was shone over the gel and the 4.2 kB fragment was excised with a scalpel (Fig. 5.3 A).

VI. Purification

The DNA fragment was extracted from the agarose and eluted in water using the QIAEXII Gel Extraction Protocol (Qiagen).

In the second cloning step, the *NPHS1* promoter was isolated from the EP_4 receptor gene located directly downstream from it. The *NPHS1* promoter was then converted into a sticky-blunt piece as was done in step 1. Cutting the plasmid with *Xho1* excised the 1.5 kB EP_4 receptor from the plasmid. A reaction mixture of 30 µl containing plasmid (1µg), NEB Buffer 2 (1x), BSA (1x), ddH_20 and *XhoI* (1:15) was incubated at 37 °C for 4 hours. These sticky ends were then blunted (II) and purified (III) as in step 1. (IV) One blunt end was converted to sticky by further cutting *RsrII*. The reaction mixture containing the plasmid (40µl eluate), NEB Buffer 4, BSA (1x) and *RsrII* was incubated at 37°C for 4 hours. (V) The reaction was then loaded onto a 1.5% agarose gel. Three segments of digested DNA were revealed: backbone containing *NPHS1* promoter, a 1.8 kB drop-out at *RsrII* and *XhoI* sites, and a 1.5 kB drop-out containing the EP_4 receptor gene. (VI) Excision, isolation and purification of plasmid backbone was done as in step 1 (Fig. 5.3 A).

Figure 5.3. Isolation of vector and insert with gel electrophoresis. (A) Left, excision of vector (*NPHS1* promoter, 11.8 kB) following *XhoI* digest, blunt and *RsrII* digest. Right, excision of insert (*2xHA-TPr*^{mut} construct, 4.2 kB) following *BamHI* digest, blunt and RsrII digest. (B) Purified samples of excised vector and insert prior to ligation (ladder= 1kB plus).

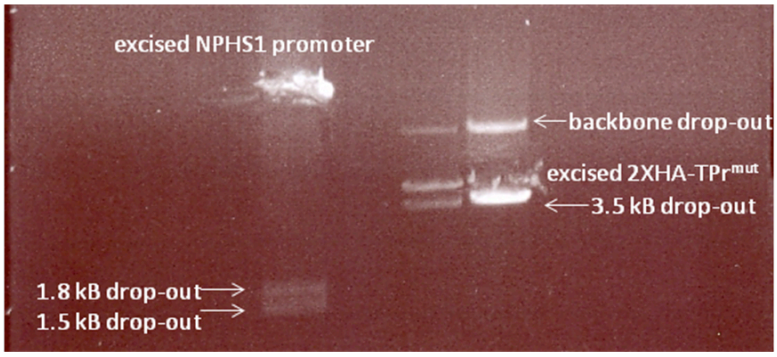
excised NPHS1 promoter
backbone drop-out
excised 2XHA-TPr^mut
3.5 kB drop-out
1.8 kB drop-out
1.5 kB drop-out

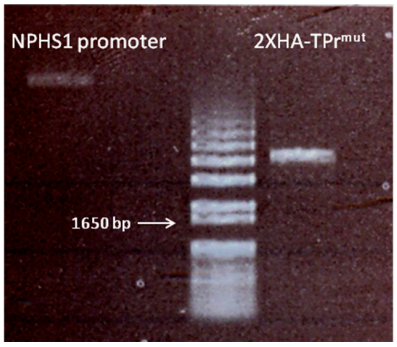
NPHS1 promoter
2XHA-TPr^mut
1650 bp

After both vector (*NPHS1*) and insert (*2XHATPr^{mut})* were prepared, the concentration of each was estimated using agarose gel electrophoresis by comparing brightness of each to the 1650 bp band of 1 kB Plus DNA ladder of known concentration (Fig. 5.3 B). We used a 3:1 ratio of vector to insert and the equations below to calculate the optimal volumes of both vector and insert DNA for the ligation reaction.

6 µl of ladder loaded = ~ 50 ng of 1650 band

Vector
50 ng x 0.5 (half as bright as 1650 band)
4.5 µl loaded
c = 5.5 ng/µl
c= m/v

5.5= 100 ng (desired mass)/v
v = 18 µl

Insert
50 ng x 1 (equal brightness)
4.5µl loaded
c= 11 ng/µl
100 ng vector x 4.2 kB insert x 5 (desired ratio)
11.8 kB vector 1

= 178 ng
c = m/v
11 ng/ µl = 178 ng / v
v = 16 µl

A 40 µl ligation reaction mixture consisting of 16 µl of insert, 18 µl of vector, 2 µl of T4 ligase and 4 µl of 10X T4 DNA ligase buffer (Promega) was incubated overnight, at 16°C.

5.1.5. Selecting clones of interest II

The methods of *Selection of clones of interest I* were repeated for the ligated plasmid. DH5α cells were once again transformed, 24 colonies were selected, amplified, harvested, lysed and plasmids were isolated. Two diagnostic tests were run to discern which clone took up the ligated plasmid. We cut the ligated plasmid with *EcoRI* and performed gel electrophoresis. We anticipated a 2.4 kB drop-out and discovered one clone (no.7) out of fifteen expressing this fragment (Fig. 5.4 A). A second diagnostic test reaction revealed the same desired pattern of fragmentation from no. 7 clone. Cutting the ligated plasmid with enzymes *SacII* and *HpaI*, showed three drop-outs of expected sizes 3.2 kB, 2.3 kB and 1.2 kB (Fig. 5.4 B).

Figure 5.4. PCR products from clones with gel electrophoresis. Two diagnostic digests reveal desired pattern of fragmentation for a successfully ligated plasmid in one clone (no. 7) out of 15. (A) A single 2.4 kB drop-out following *EcoRI* digestion. (B) Three drop-outs of sizes 3.2 kB, 2.3 kB and 1.2 kB following *SacII* and *HpaI.*

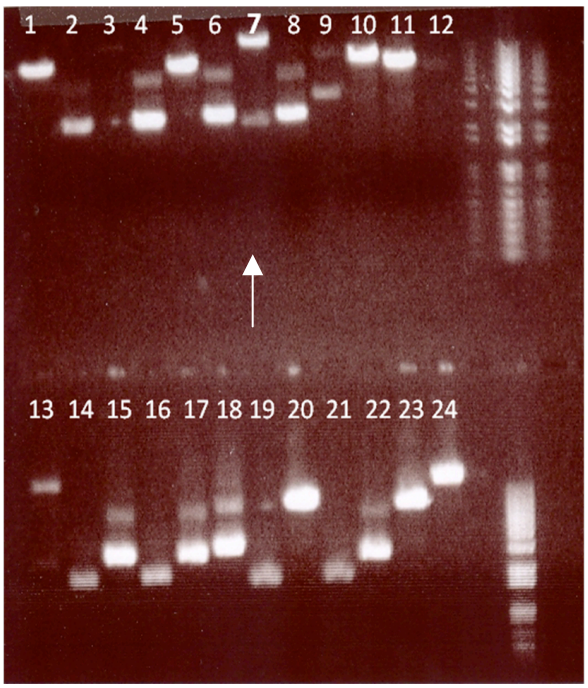
1 2 3 4 5 6 7 8 9 10 11 12
13 14 15 16 17 18 19 20 21 22 23 24

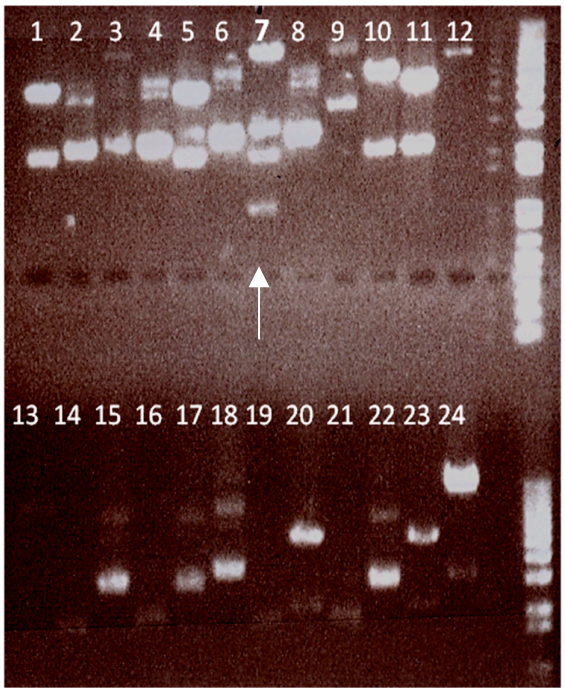
1 2 3 4 5 6 7 8 9 10 11 12
13 14 15 16 17 18 19 20 21 22 23 24

5.1.6. DNA Sequencing

The plasmid was sequenced to ensure it was correct and free of mutation along the ligation junctions (Sprott Centre for Stem Cell Research, Applied Biosystems 3730 DNA Analyzer). The custom *NPHS1* promoter antisense primer CKNE11 (5'GAGAAAGAACTGTTAACGGG3') was anticipated to bind to and sequence (in the 5' to 3' direction) the last few hundred base pairs of the *NPHS1* promoter, as well as the first few hundred base pairs of the anticipated ligated TPr^{mut} insert. To sequence the TPr^{mut} insert in 3' to 5' direction, we took advantage of the commercially available *SP6* promoter primer (5´ATTTAGGTG ACACTATAG3') which is complementary to a portion of the SP6 RNA Polymerase promoter found in pcDNA3 downstream from our potential TPr^{mut} insert.

The nucleotide sequence obtained was 'blasted' against the *Mus musculus* genome (strain C57BL/6J) using the NCBI online BLAST program: http://www.ncbi.nlm.nih.gov/genome/seq/BlastGen/BlastGen.cgi?taxid=10090 Portions of the plasmid sequenced by CKNE11 were identified by BLAST as NPHS1 and TPr. Going in the 5' to 3' direction, the last 182 base pairs of the *NPHS1* promoter and the beginning 244 base pairs of TPr^{mut} were sequenced with 100% and 99% similarity, respectively, to the database genome.

The portion of the plasmid sequenced by SP6 was identified as TPr. Going in the 5' to 3' direction, the last 183 base pairs of TPr^{mut} were sequenced with 95% similarity to the database genome (Fig. 5.4). Although the entire span of the ligated

plasmid was not sequenced, the high degree of similarity of the sequenced regions with the database genome was deemed satisfactory.

Figure 5.5. Genomic sequencing of *NPHS1-2xHA-TPr^{mut}* construct. DNA segments are not to scale. Following DNA sequencing with CKNE11 and SP6 primers, segments of both NPHS1 promoter and *TPr^{mut}* were matched to an online BLAST database genome identifying them as belonging to *NPHS1* and *TPr*. Going in the 5' to 3' direction, the last 182 base pairs of the *NPHS1* promoter were sequenced, and the beginning 244 base pairs of TPr^{mut} with 100% and 99% similarity, respectively, to the database. The last 183 base pairs of *TPr^{mut}* were sequenced with 95% similarity to the database.

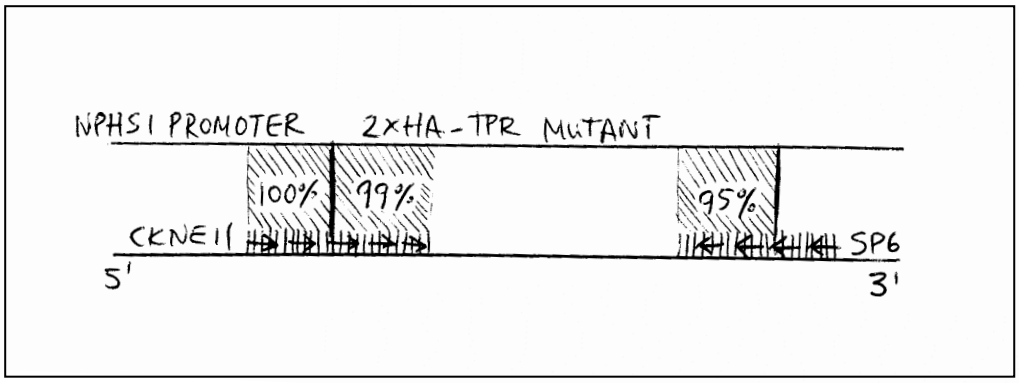
NPHS1 PROMOTER
2×HA-TPR MUTANT
100%
99%
95%
CKNE11
SP6
5'
3'

CKNE11:

```
Features in this part of subject sequence:
   nephrosis 1 homolog, nephrin

 Score =  337 bits (182)  Expect = 1e-89
 Identities = 182/182 (100%), Gaps = 0/182 (0%)
 Strand=Plus/Plus

Query  1-60      CGATGCCGGGACAGAAAGACTGCGACAGTCACAGACAATGGTaggaagataagagaaaga
                 ||||||||||||||||||||||||||||||||||||||||||||||||||||||||||||
Sbjct  28244982  CGATGCCGGGACAGAAAGACTGCGACAGTCACAGACAATGGTAGGAAGATAAGAGAAAGA  28245041

Query  61-120    aggaagggagggagggagggagggaagagagaagggcgagttagaaagagattgaaagaa
                 ||||||||||||||||||||||||||||||||||||||||||||||||||||||||||||
Sbjct  28245042  AGGAAGGGAGGGAGGGAGGGAGGGAAGAGAGAAGGGCGAGTTAGAAAGAGATTGAAAGAA  28245101

Query  121-180   cagaaaagCAGGGCACACAGAGAGAGGCTCAGGGAAGACAGCAACAAACAAGCTGCTGGT
                 ||||||||||||||||||||||||||||||||||||||||||||||||||||||||||||
Sbjct  28245102  CAGAAAAGCAGGGCACACAGAGAGAGGCTCAGGGAAGACAGCAACAAACAAGCTGCTGGT  28245161

Query  181       GA  182
                 ||
Sbjct  28245162  GA  28245163


Features in this part of subject sequence:
   thromboxane A2 receptor

Score =  446 bits (241)  Expect = 2e-122
 Identities = 243/244 (99%), Gaps = 0/244 (0%)
 Strand=Plus/Plus


Query  259-318   TGGCCCTATGGCACCTCGCTGGGGGCCTGCTTTCGCCCGGTGAACATCACGCTGCAGGAG
                 |||||| ||||||||||||||||||||||||||||||||||||||||||||||||||||
Sbjct  23126614  TGGCCCAATGGCACCTCGCTGGGGGCCTGCTTTCGCCCGGTGAACATCACGCTGCAGGAG
23126673

Query  319-378   CGACGTGCCATCGCGTCGCCATGGTTCGCTGCGTCCTTTTGCGCGCTGGGCCTGGGGTCC
                 ||||||||||||||||||||||||||||||||||||||||||||||||||||||||||||
Sbjct  23126674  CGACGTGCCATCGCGTCGCCATGGTTCGCTGCGTCCTTTTGCGCGCTGGGCCTGGGGTCC
23126733

Query  379-438   AACCTGCTGGCACTGAGTGTGCTGGCTGGGGCGCGGCCCGGCGCGGGACCCCGCTCCTCC
                 ||||||||||||||||||||||||||||||||||||||||||||||||||||||||||||
Sbjct  23126734  AACCTGCTGGCACTGAGTGTGCTGGCTGGGGCGCGGCCCGGCGCGGGACCCCGCTCCTCC
23126793

Query  439-498   TTCCTCGCTCTGCTGTGCGGCCTTGTTCTCACCGACTTCCTGGGGCTGCTAGTCACCGGC
                 ||||||||||||||||||||||||||||||||||||||||||||||||||||||||||||
Sbjct  23126794  TTCCTCGCTCTGCTGTGCGGCCTTGTTCTCACCGACTTCCTGGGGCTGCTAGTCACCGGC
23126853

Query  499       GCCA  502
                 ||||
Sbjct  23126854  GCCA  23126857
```

SP6:

```
Features in this part of subject sequence:
   thromboxane A2 receptor

 Score =  289 bits (156),  Expect = 3e-75
 Identities = 174/183 (95%), Gaps = 0/183 (0%)
 Strand=Plus/Plus


Query  503-562   GGGCCACAGAGCACCAGCTGCTCATCTACATGCGTGTAGCCACCTGGAACCAGATCTTGG
                 ||||||||||||||||||||||||||||| ||||||| ||||||||||||||||||||||
Sbjct  23128655  GGGCCACAGAGCACCAGCTGCTCATCTACCTGCGTGTGGCCACCTGGAACCAGATCTTGG
23128714

Query  563-622   ACCCCTGGGTCTATATCCTCATTAGCCGGTCTGAGCTCCGGCGCCTGCATCCGCGGTTCG
                 |||||||||||||||||| || ||||||||| |||||||||||||||||||||||||||
Sbjct  23128715  ACCCCTGGGTCTATATCCTCTTTCGCCGGTCTGTGCTCCGGCGCCTGCATCCGCGGTTCA
23128774

Query  623-682   GTGCACAGCTACAGGCTGTGGCCTTGCGCCGGCCTCCAGCCCAGGCCATGCTCAGTGGAC
                 || ||||||| ||||||||| ||||||||||||||||||||||||||||||||||||||
Sbjct  23128775  GTTCACAGCTCCAGGCTGTGTCCTTGCGCCGGCCTCCAGCCCAGGCCATGCTCAGTGGAC
23128834

Query  683       CCT  685
                 |||
Sbjct  23128835  CCT  23128837
```

5.1.7. Preparing DNA for transgenesis

The *NPHS1-2xHA-TPr*^{mut} construct was subsequently linearized with FspI and *HindIII*. A reaction mixture of 30 µl containing plasmid (10µg), NEB Buffer 2 (1x), BSA (1x), water, *FspI* (1:15) and *HindIII* (1:15) was incubated at 37°C overnight. The DNA was run on a 0.8% agarose gel. A 2.3 kB and a 1.5 kB fragment dropped out, part of the unwanted pcDNA backbone. The 12.2 kB fragment containing the construct was excised with a scalpel and purified using the Qiagen gel extraction kit. DNA was eluted from the column with Tris-EDTA buffer pH 8.0. Using gel electrophoresis, DNA concentration was estimated by comparing to the thickness of the 1650 band of known concentration of 10ng/µl. DNA was diluted with 1x PBS to

50µl of 5ng/µl DNA. DNA was spun for 20 minutes at high speed then spun again in an equilibrated Centrex column for 10 minutes, 22°C, 2800 rpm.

5.2. TRANSGENIC MOUSE DEVELOPMENT

The principles of transgenic mouse development are outlined below as performed by Yves de Repentigny, senior research assistant at the Ottawa Hospital Research Institute and technologist Adriana Gambarotta at the Transgenic Unit of the Animal Care Facility at the Ottawa Hospital Research Institute (Civic Campus)[37].

5.2.1 Superovulation

The recovery of large numbers of preimplantation embryos is required for microinjections of eggs. Pregnant mare's serum gonadotropin (PMSG) is used to mimic follicle-stimulating hormone (FSH) and human chorionic gonadrotropin (hCG) to mimic luteinizing hormone (LH). Efficient induction of superovulation in donor females depends on several variables including age and weight of females, dose of gonadotropins and time of administration and the strain of mice. In addition, the number of superovulated eggs that actually become fertilized depends on the reproductive performance of the stud males.

5.2.2. Matings

Superovulated donor females are paired with stud males, and the next morning females are checked for a copulation plug. In conjunction, sterile vasectomized males are paired with separate females who will act as pseudopregnant recipients. Following successful copulation plug formation, these females will undergo a physiological change in the uterus that will promote implantation of the transgenic embryos.

5.2.3. Egg collection

Flushing out the oviduct of superovulated females collects fertilized eggs. Hyaluronidase removes the surrounding cumulus cell layer, and the eggs are incubated in a microdrop embryo culture in preparation for microinjection.

5.2.4. Microinjection

DNA is directly injected into the pronuclei of fertilized mouse eggs leading to the stable chromosomal integration of the foreign DNA at the one-cell stage. Sites of integration into the genome are unpredictable and the number of copies integrated per cell can vary from one to several hundred.

5.2.5. Embryo transfer

Following incubation, embryos are transferred into the reproductive tract of recipient pseudopregnant females bilaterally using the infundibular opening of the oviducts.

5.2.6. Offspring analysis

Upon weaning pups, tail or ear snip are screened for transgene expression using CKNE11, (5'GAGAAAGAACTGTTAACGGG3') and a custom TPr antisense primer (5'ACGTCGCTCCTGCAGCGTGA-3').

Senior research assistant Yves de Repentigny at the Ottawa Hospital Research Institute performed the first three rounds of transgenic mouse development. The protocol was as follows:

Day 1. Preparation of mice for microinjection

Female donors were used at 5-6 weeks of age; they were injected intraperitoneally with 100µl of PMSG (5I.U./100µl) 48 hours prior to the mating and with 100µl of hCG (5I.U./100µl) on the day of the mating with fertile studs. Female recipients in estrus are chosen from a pool of CD1 females at 8 weeks of age and mated on the same day with sterile CD1 males.

Day 2. Egg collection, microinjection and embryo transfer

Embryos were collected from the donors. Fertilized egg cells are microinjected at the one-cell stage with DNA (2ng/µl), purified by using Whatman Centrex 0.2µm cellulose acetate filter. All surviving injected embryos are stabilized at +37˚C in M-16 media with amino acids overnight, and are then transferred to the reproductive system of plugged embryo recipients.

Day 23. Offspring analysis

Approximately twenty-one days after the transfer, the embryo recipients gave birth to pups. Pups were weaned at three weeks of age, ear tagged and screened by using small portions of ear lobes. After weaning, pups were tagged, tailed and genotyped using the REDExtract-N-Amp Tissue PCR Kit (Sigma-Aldrich) according to manufacturer's instructions. Primers were designed to amplify a 325 bp-long segment between the TPr gene (5' ACGTCGCTCCTGCAGCGTGA 3') and the NPHS1 promoter gene (5'GAGAAAGAACTGTTAACGGG3').

The fourth round was carried out by technologist Adriana Gambarotta at the Transgenic Unit of the Animal Care Facility at the Ottawa Hospital Research Institute (Civic Campus). The protocol was as follows:

Day 1. Preparation of mice for microinjection

Female donors were used at 4-5 weeks of age; they were injected intraperitoneally with 50µl of PMSG (5I.U./100µl) 48 hours prior to the mating and with 50µl of hCG (5I.U./100µl) on the day of the mating with fertile studs. Female recipients in estrus are chosen from a pool of CD1 females at 8-12 weeks of age and mated on the same day with sterile CD1 males.

Day 2. Egg collection, microinjection and embryo transfer

Embryos were collected from the donors. Fertilized egg cells are microinjected at the one-cell stage with DNA (5ng/µl), purified by using Whatman Centrex 0.2µm cellulose acetate filter. All surviving injected embryos are stabilized at +37˚C in KSO media with amino acids for at least an hour, and are then transferred to the reproductive system of plugged embryo recipients.

Day 23. Offspring analysis

Approximately twenty-one days after the transfer, the embryo recipients gave birth to pups. Pups were weaned at three weeks of age, ear tagged and screened by using small portions of ear lobes. After weaning, pups were tagged, tailed and genotyped as described in previous protocol by Y. de Repentigny.

5.3. CHARACTERIZATION

5.3.1. Urinalysis

Morning spot urine samples were collected and albumin levels were assayed with Albuwell M Test Kit according to manufacturer's instructions; a 1:80 dilution of urine was employed (Exocell). Results were corrected for urine creatinine content with the Creatinine Companion kit (Exocell).

5.3.2. RNA Extraction and Quantitative RT-PCR

I. Purification of RNA from kidney

Mice were anaesthetized with isofluorane and perfused with 1x PBS delivered through left ventricle with a syringe. Kidneys were removed, decapsulated, poles removed, and remaining kidney was halved medially, one-half being snap frozen in liquid nitrogen. RNA was isolated using the RNeasy Mini Kit (Qiagen) according to manufacturer’s instructions.

II. DNA synthesis

The purified RNA sample was additionally cleared of contaminating genomic DNA and reverse transcription was carried out using the Quantitect Reverse Transcription Kit (Qiagen) according to manufacturer’s instructions.

III. Real-time PCR

Primers were designed to bind to the tail end of the TPr (5' CAGGCCATGCT CAGTGGAC 3') and the 3' end HA tag (Reverse primer: 5' TCAGGCGTAGTCTGG GACGT 3') so that a 12-base pair target spanning both TPr sequence and HA tag would be amplified. PCRs were performed in 25-ml volumes, using MicroAmp vials, as follows. The PCR reaction mixture consisted of cDNA (~50 ng), MgCl2 (2.5 mM); primers (5 μM), Quantitect SYBR Green PCR Master Mix (1x) (Quantitect SYBR Green PCR Kit, Qiagen) Probe. A thermocycler (ABI Prism 7000 SDS) was used for amplification. All cycles began with 2 min at 50°C and then 10 min at 95°C. Following these initial steps, two-step cycles were 15 s at 95°C and 60 s at 60°C. All reactions were performed in triplicate. All values were normalized to rodent glyceraldehyde-3-phosphate dehydrogenase (GAPDH) (Forward primer: 5' GCAAA GTGGAGATTGTTGCCAT 3', reverse primer: 5' CCTTGACTGTGCCGTTGA ATTT3', Invitrogen). Standard curves were performed for both TPr^{mut} and GAPDH primers at 12.5, 6.25, 3.125, 1.56 ng/μl concentrations.

5.3.3. Immunofluorescence

Mice were anaesthetized and perfused with a 1x PBS perfusate, delivered through the left ventricle with a syringe. Kidneys were removed, decapsulated, poles removed, and remaining kidney was halved medially, one-half being fully immersed in OCT medium and plunged repeatedly in liquid nitrogen until frozen and then

placed on dry ice. Frozen kidney was delivered to University of Ottawa Pathology for sectioning. Slides were stored in -20°C until immunofluorescence was performed. Slides were rinsed in 1X PBS, dried and the Immedge pen was used to create a waterproof border around the section. Section was blocked with 5% goat serum in PBS for 1 hour at room temperature in a humidified chamber. Blocking solution was then aspirated and slides were treated with the primary antibody (1:100) in 2% goat serum in PBS. Slides were incubated overnight at 4°C in a humidified chamber. The following day, the antibody solution was aspirated and the slide was rinsed in PBS. The secondary anti-rabbit antibody solution was applied (2% goat serum in PBS). Slides were incubated at room temperature for 1 hour in a humidified chamber. The secondary was aspirated and the slides were rinsed in PBS and dried. Tissue section was treated with one drop of fluoromount G mounting media, covered with glass cover slips and sealed with nail polish.

5.3.4. Renal histology

Periodic acid-Schiff and hematoxylin and eosin staining was performed by the University of Ottawa Pathology department on kidney sections fixed in 4% paraformaldehyde in PBS. Sections were assessed for glomerular damage under light microscope (Zeiss).

5.3.5. Dynabead perfusion and glomerular isolation

A method for the isolation of mice glomeruli using spherical Dynabeads has been developed and described by Takemoto and colleagues[38]. Dynabeads are composed of a monodisperse polymer, demonstrating magnetic properties within a magnetic field. Dynabeads are fitted to specifically embolize glomerular capillaries.

Mice were anaesthetized and perfused with a 1x PBS perfusate containing rinsed dynabeads through the left ventricle with a syringe. Kidneys were removed, decapsulated, finely minced with a scalpel and placed in Hank's balanced salt solution (HBSS) solution containing collagenase (1mg/ml) and DNAse (0.1 mg/ml) on ice. Kidneys were then incubated in 37°C bath for 30 minutes to promote digestion. Kidneys were then ground through a 100 μm sieve, the sieve was rinsed with a further 5 ml of HBSS and the solution was collected in a Falcon tube subsequently centrifuged for 5 min at 700 rpm. Supernatant was removed and pellet resuspended. Glomeruli within pellet were collected using a magnet, rinsed 3 times with HBSS, centrifuged and resuspended in media for subsequent stimulation.

5.3.6. Glomerular stimulation

Isolated glomeruli were suspended inmedia and stimulated with either vehicle (methyl acetate) or U-46619, a stable analog of the prostaglandin H_2, and a TP receptor agonist, exhibiting similar properties to thromboxane A_2. Glomeruli were stimulated for 2 h (mRNA) and 6 h (protein) at 37°C in serum-

deprived media (0.1 % FBS) and then harvested. For protein extraction, cells were lysed with protease-containing RIPA buffer and western blot was performed for COX-2. RNA was isolated using the RNeasy Micro Kit (Qiagen) according to manufacturer's instructions.

5.4. CELL CULTURE

Mature podocytes are mitotically arrested, requiring special cell culture conditions to replicate the specialized and terminally differentiated phenotype *in vitro*. To generate large numbers of cells, cells are first grown under growth permissive conditions, where immortalized podocytes replicate. Growth media consists of RPMI 1640 containing 10% fetal bovine serum supplemented with 20–100 U/ml of mouse interferon gamma (INF-γ) to drive T-antigen expression. The culture dishes are coated with type I collagen to promote podocyte proliferation. As the tsA58 mutant T antigen is temperature sensitive, a culture temperature of 33°C is required. To silence the tsA58 T antigen, thereby inducing cell cycle exit and differentiation, the cultures are then switched to medium lacking INF-γ and transferred to an incubator set at 37°C. The removal of INF-γ from the culture media results in the loss of IFN-γ-driven H-2Kb-promotor activity and the higher temperature of 37°C causes the degradation of the remaining tsA58 T antigen. Podocytes used for *in vitro* work were a gift of S. Shankland of the University of Washington, Seattle, WA.

Unless otherwise specified, podocytes were serum-deprived for 48 hours prior to experimental manipulation.

5.5. MECHANICAL STRETCH AND HIGH GLUCOSE

Podocytes were grown on collagen I coated silicone membranes of 6-well BioFlex plates and set up in the Flexercell FX-4000T apparatus (Flexcell Int.). A vacuum was applied to the plates to create a cyclical sinusoidal pattern of equibiaxial stretch of 10 % at a frequency of 0.5 Hz. High glucose was a 25 mM solution of D-Glucose while control was 5 mM of D-Glucose and 20 mM of L-Glucose to control for osmolarity.

5.6. TXB_2 ASSAY

Because TxA_2 is rapidly hydrolyzed non-enzymatically to form TXB_2 metabolites, measurement of TXB_2 gives more accurate estimates of *in vivo* TxA_2 production. Media was collected from cell culture and TXB_2 levels were assayed by EIA according to manufacturer's instructions (Thromboxane B_2 EIA Kit, Cayman Chemical). TXB_2 levels were expressed relative to protein levels quantified using the BCA protein assay kit (Thermo Scientific,) according to manufacturer’s instructions.

5.7. HPLC

Superoxide assessment was performed for cultured cells and incubated with dihydroethidium (DHE) as a probe for superoxide, followed by acetonitrile extraction and HPLC analysis of fluorescent products obtained from DHE oxidation (ethidium and 2-hydroxyethidium). Cells were washed with PBS/100 mM DTPA three times. HBSS containing DTPA (100 mM) was added to each well, followed by DHE (50 mM). Cells were incubated for 30 minutes and then washed three times with PBS/DTPA. Cells were harvested by scraping with acetonitrile. Lysates were centrifuged (12,000g, 10 min), and supernatants were transferred to an Eppendorf tube and acetonitrile dried under vacuum for 2 to 3 h (DNA Speed-Vac Concentrator, Thermo Savant). For HPLC analysis, samples were resuspended in 120 ml PBS/DTPA, and a volume of 100 ml was injected (Agilent 1100 Series).

5.8. APOPTOSIS STUDIES

5.8.1 Annexin-V FITC

Differentiated podocytes (14 days of differentiation) were seeded onto collagen I-coated 10 cm petri dishes. Podocytes were incubated with 1 μM U-46619 in RPMI containing 0.1% FBS for 24 hours in the presence of 5 μM indomethacin (to block endogenous prostanoid production). Serum-deprived cells were exposed to identical experimental conditions but without U-46619. The control group was given

media with regular, 10% FBS instead of 0.1%. After 24 hours, cells were trypsinized, labeled with Annexin-V and propidium iodide (PI) according to manufacturer's instructions (Apotarget Annexin-V FITC Apoptosis kit, Invitrogen) and analyzed by flow cytometry (FC500 Beckman Coulter).

5.8.2. Hoescht 33342

Differentiated podocytes (14 days of differentiation) were seeded onto 15 mm circular coverslips (Fisher) placed in Multiwell^{TM} -12 well collagen I-coated plates (Multiwell, Falcon). Experimental conditions were identical to those in the Annexin-V FITC Assay. After 24 hours, coverslips with adherent podocytes were collected, washed and fixed in acetone-methanol and stained with Hoechst 33342 for 20 minutes at room temperature. Coverslips were washed again, mounted on glass slides, and podocytes were quantified by fluorescent microscope. Two coverslips were used per experimental group, with at least 300 being counted on each slide. The Hoechst 33342 dye stains morphologically normal nuclei a diffuse pale blue, whereas apoptotic nuclei demonstrate condensed, smaller, and very intensely bright blue nuclei.

5.8.3. TUNEL

In situ detection of DNA fragments was performed using fluorescein cell death detection kit (Roche). Tissue was fixed with 4% paraformaldehyde, washed with

PBS and treated with a TUNEL reaction mixture 45 minutes at 37°C. Slides were washed in PBS and coverslipped with Fluoromount G mounting medium (Electron Microscopy Sciences). Positive cells were counted with fluorescent microscope at 630x (Zeiss).

5.9. WESTERN BLOT ANALYSIS OF COX-2 EXPRESSION

Western blot analysis was performed to quantitate COX-2 protein levels. Briefly, protein extracts in Laemmli buffer containing 5% β-Mercaptoethanol were separated by sodium dodecyl sulfate–polyacrylamide (SDS) gel electrophoresis and transferred to a nitrocellulose membrane (Bio-Rad). After blocking non-specific binding with 5% non- fat dry milk or 5% bovine serum albumin (Sigma-Aldrich), membranes were incubated overnight at 4°C with COX-2 (murine) Polyclonal primary antibody (Cayman). HRP-conjugated donkey anti-rabbit secondary antibody (Jackson ImmunoResearch) was applied for 1 hour at room temperature followed by enhanced chemiluminescence (ECL) western blotting system (Thermo Scientific). Blots were stripped and reprobed using the same protocol, however β-actin anti-rabbit antibody was used as the primary (Sigma-Aldrich).

5.10. STATISTICAL ANALYSIS

All experimental data were analyzed using GraphPad PRISM software. Data are expressed as means ± SEM. One-way ANOVA test followed by Tukeys multiple comparison test was used when appropriate.

6. RESULTS

6.1. IN VITRO

6.1.1. TPr agonism undermines podocyte viability

To evaluate the role of TPr agonism on cell viability, cultured podocytes were treated with U-46619 for 24 hours and apoptosis was quantified using three methods, Annexin-V FITC, Hoescht 33342 and TUNEL labeling. The TPr agonist, U-46619 (1 μM) provoked a three-fold increase in apoptosis in podocytes labeled with Annexin V-FITC compared to control and starved groups (Fig. 6.1). Hoescht staining revealed approximately 20% of podocytes treated with U-46619 were apoptotic compared to 4% and 8% of control and starved groups, respectively (Fig.6.2, Fig. 6.3). Finally, TUNEL staining revealed a similar, although non-significant trend (Fig. 6.4).

Figure 6.1. TPr agonism and apoptosis in culture podocytes (flow cytometry). Results are presented as mean ± SEM (n=5) and are expressed as fold increase of control. The TPr agonist, U-46619 (1 μM, 24 h) elicited a ~3 fold increase in apoptosis vs. control and starved groups ($p < 0.001$). Control group was given normal medium (10% FBS), all remaining groups were serum starved (0.1% FBS). Cells staining for annexin-V fluorescein iso-thiocyanate (FITC) conjugate only were counted as apoptotic (FC500 Flow Cytometer, Beckman Coulter).

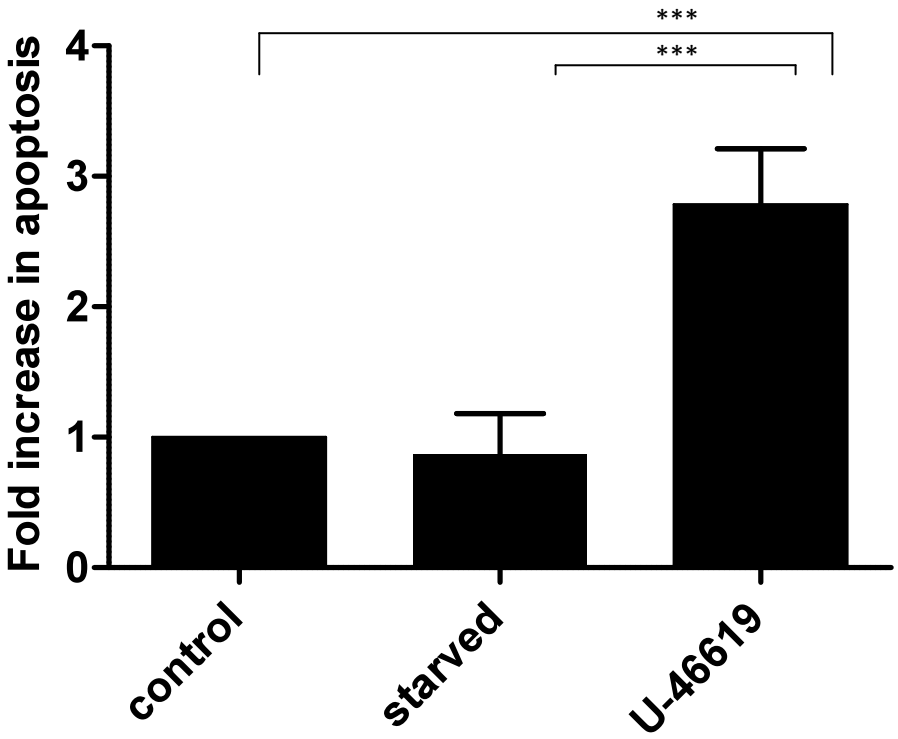
***
***
Fold increase in apoptosis
4
3
2
1
0
control
starved
U-46619

Figure 6.2. TPr agonism and apoptosis in cultured podocytes (Hoescht). Results are presented as mean ± SEM (n=3) and are expressed as % of total nuclei. 20% of podocytes treated with U-46619 were apoptotic, compared to 4% in control, and 8% in starved groups ($p<0.001$). Cells were stained with Hoechst 33342 for quantification under fluorescence microscopy. Two coverslips were used per experimental group, with at least 300 cells being counted/slide.

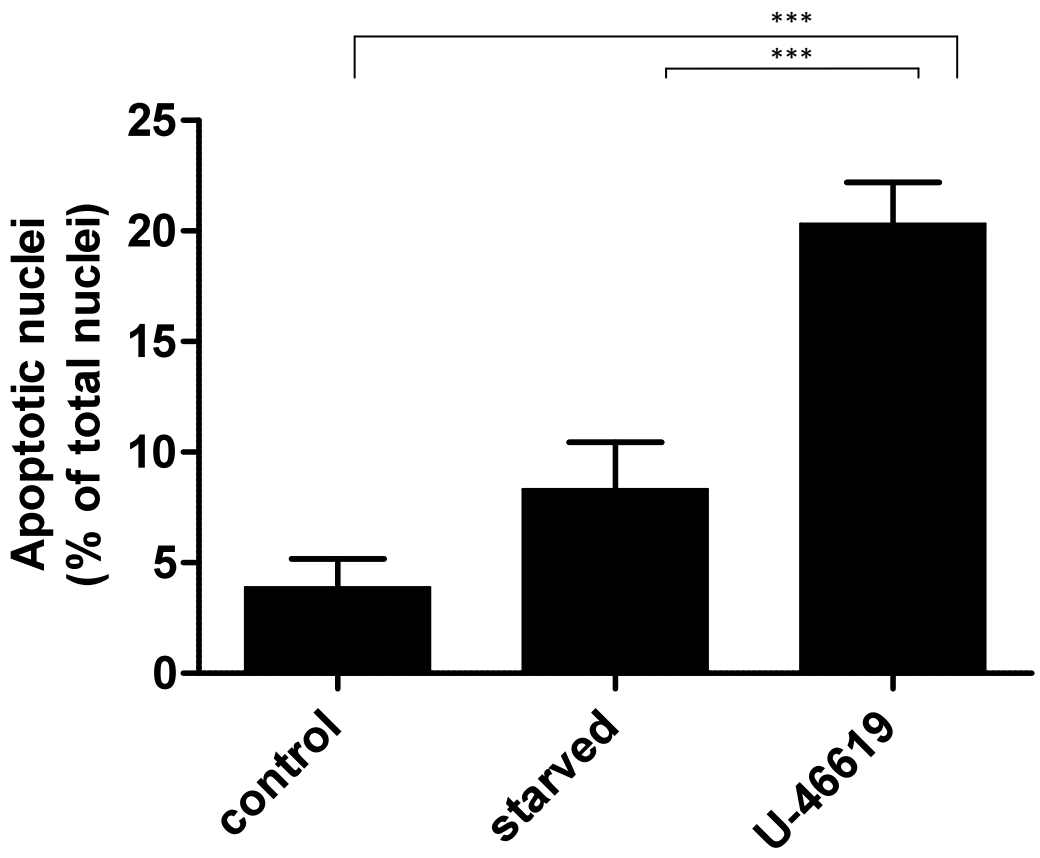
***
***
Apoptotic nuclei
(% of total nuclei)
25
20
15
10
5
0
control
starved
U-46619

Figure 6.3. Hoescht 33342 staining of cultured podocytes. (A) Podocytes stained with Hoescht 33342 from U-46619-stimulated group showing apoptotic body (arrow). (B) Control group. Cells were examined with fluorescent microscope (x630, Zeiss).

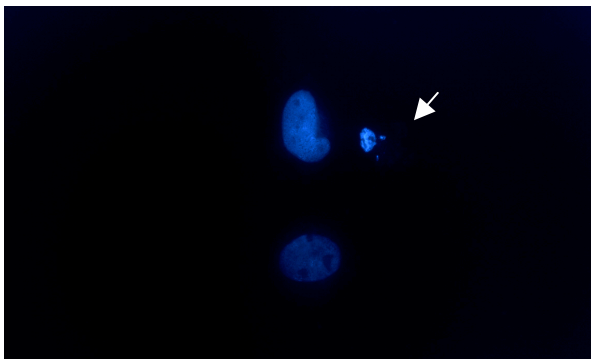

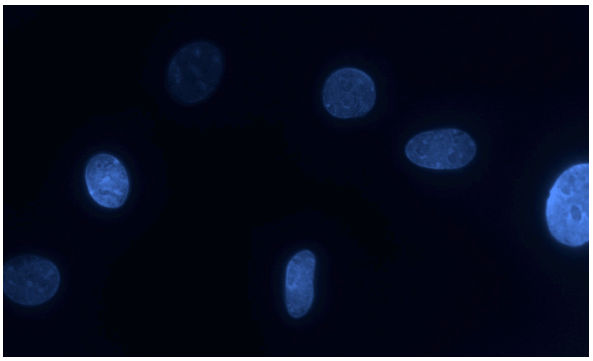

Figure 6.4. TPr agonism and apoptosis in cultured podocytes (TUNEL). Values are expressed as fraction of apoptotic nuclei over total number of nuclei, averaged over 5 observed fields. Results are presented as mean ± SEM (n=3) and as fold increase of control. Podocytes treated with U-46619 are approximately 30 times more susceptible to apoptosis as quantified by TUNEL staining (ns). Cells were examined with fluorescent microscope (x630, Zeiss).

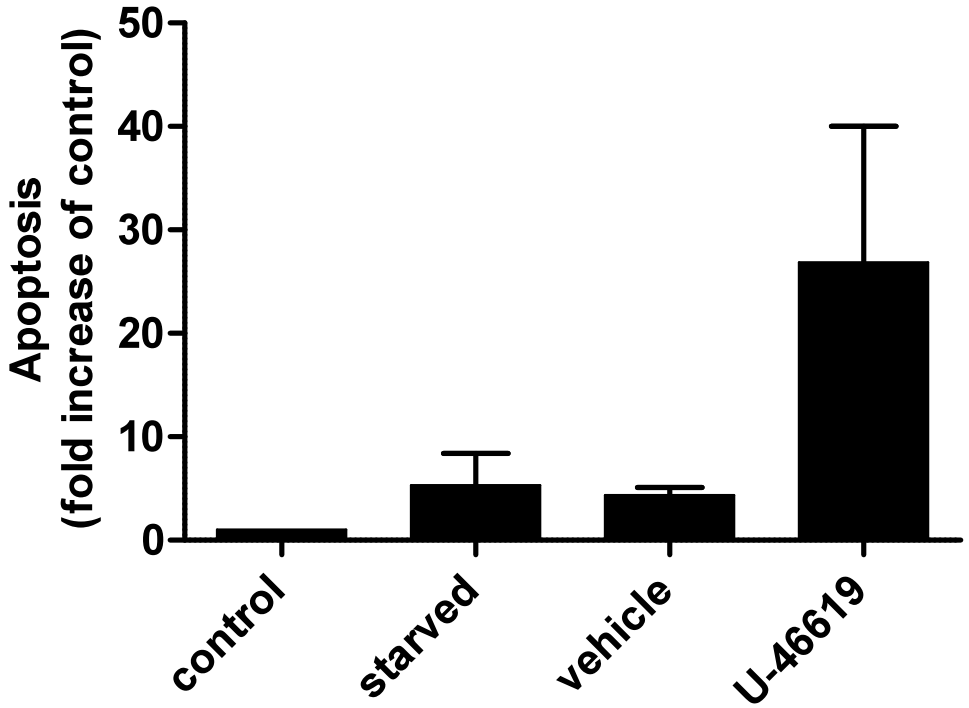
Apoptosis
(fold increase of control)
50
40
30
20
10
0
control
starved
vehicle
U-46619

6.1.2. TPr agonism does not affect viability under high glucose and stretch

Podocytes subjected to high glucose alone, mechanical stretch alone, or both do not appear more susceptible to cell death compared to the control group. Furthermore, pharmacological blockade of TPr does not enhance viability anymore compared to the control group. Podocyte apoptosis does however increase when U46619 is applied, and may be further enhanced by stretch (Fig. 6.5).

6.1.3. TPr agonism does not induce reactive oxygen species production

To determine whether TPr activity induces podocyte damage via reactive oxygen species production, an HPLC assay was performed. Podocytes stimulated with U-46619 do not appear to have enhanced superoxide production compared to control, starved and vehicle groups (Fig. 6.6).

6.1.4. TxB_2 production may be enhanced under high glucose and stretch

Podocytes were stimulated with high glucose, stretch and both to determine whether these conditions are linked to enhanced COX-2 production, and subsequent TxA_2 synthesis. This was measured using the stable metabolite, TxB2. Increased TxB2 concentrations appear (corrected against total protein) after 24-hour treatment with high glucose alone (2-fold, ns), and in concert with mechanical stretch (9-fold, ns) (Fig.6.7).

Figure 6.5. TPr agonism and apoptosis in response to conditions of high glucose and stretch. Values are expressed as fold increase of control of fraction of apoptotic nuclei over total number of nuclei, averaged over 5 observed fields. Results are presented as mean ± SEM (n=3) and as fold increase of control. Cells treated with stretch, high glucose or combination of both (24 h) were not more susceptible to cell death compared to control (ns). TPr antagonist BM-567 exerts no apparent pro-viability effect. Cells were examined with fluorescent microscope (x630).

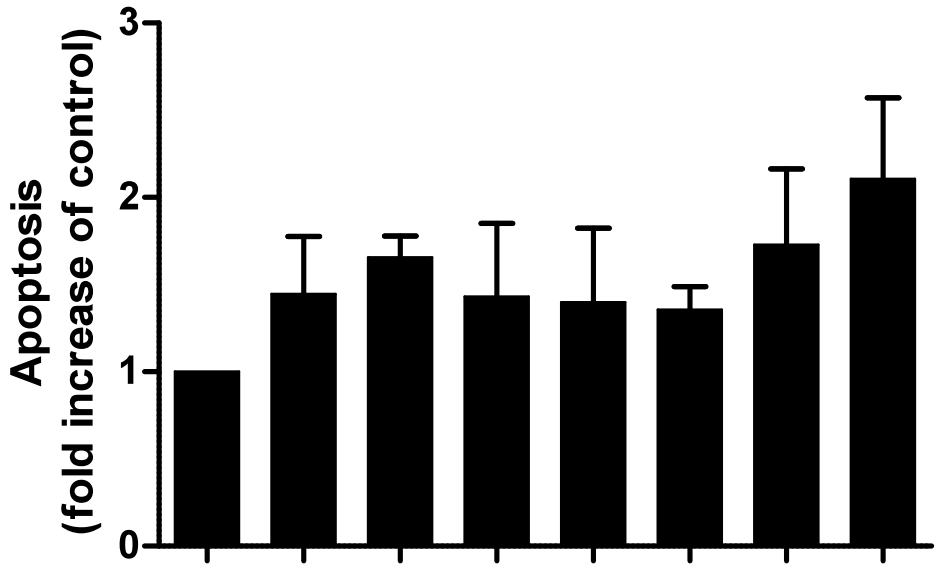

normal glucose	+	+	-	-	+	+	-	-
stretch	-	+	-	+	-	+	-	+
high glucose	-	-	+	+	-	-	+	+
BM-567	-	-	-	-	+	+	+	+

Figure 6.6. TPr agonism and superoxide production. Values are expressed as fraction of 2-hydroethidium to dihydroethidium. Results are presented as mean ± SEM (n=3). Enhanced TPr activity does appear to induce superoxide production (ns) compared to control, starved and vehicle groups. High glucose as positive control did not show significant increase compared to any groups.

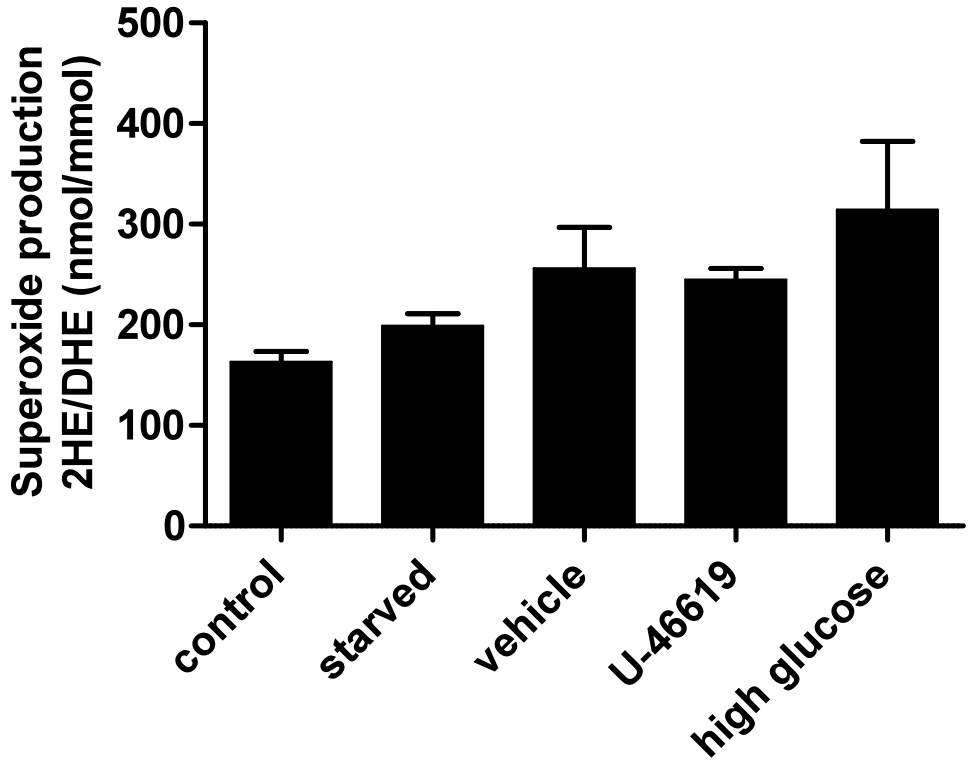
Superoxide production
2HE/DHE (nmol/mmol)
500
400
300
200
100
0
control
starved
vehicle
U-46619
high glucose

Figure 6.7. TxB_2 production in cultured podocytes in response to conditions of high glucose and mechanical stretch. Values are expressed as fold increase of control of TxB_2 concentration (pg/ml) over total cell protein (ug/ml). Results are presented as mean ± SEM (n=3). High glucose alone and in concert with mechanical stretch appear to enhance TxB_2 production compared to control with two-fold and nine-fold increases, respectively (ns).

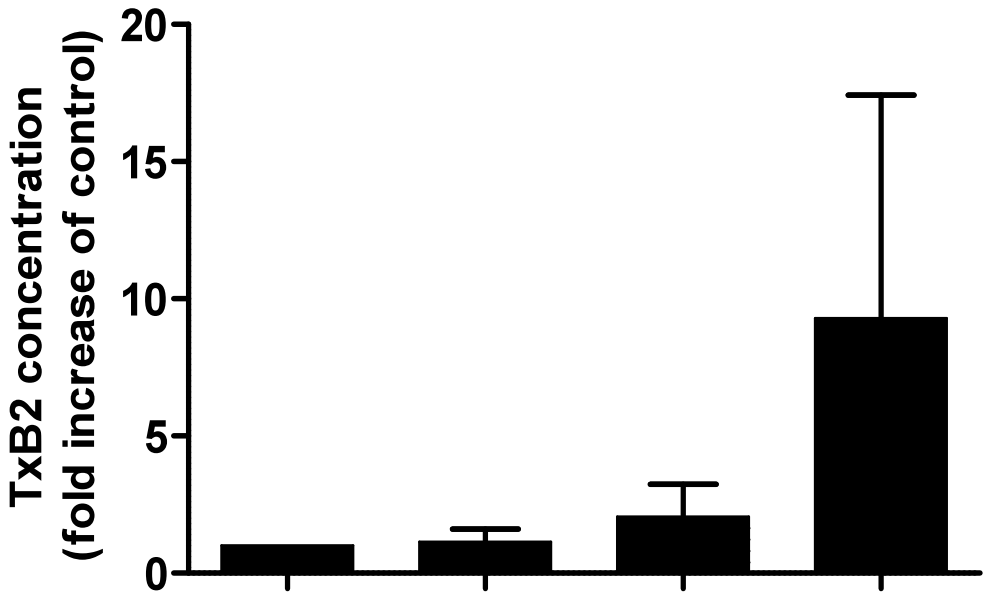

normal glucose	**+**	**+**	**-**	**-**
stretch	**-**	**+**	**-**	**+**
high glucose	**-**	**-**	**+**	**+**

6.1.5. TPr agonism may enhance COX-2 expression in cultured podocytes

To determine whether stimulation of TPr induces COX-2 expression, COX-2 protein levels were measured by western blot following 6 hour stimulation with U-46619 and respective controls. TPr agonism appears to enhance COX-2 levels (2.5-fold, ns), while stimulation with positive control PGE_2, enhances COX-2 levels significantly compared to control (3.2-fold, $p<0.05$) (Fig. 6.8).

Figure 6.8. TPr agonism and COX-2 production in cultured podocytes. (A) Values are expressed as fold increase of control using arbitrary densitometric units of COX-2 corrected with β-actin. Results are presented as mean ± SEM (n=3). TPr agonism appears to enhance COX-2 protein levels compared to control (2.5-fold, ns). (B) Representative western blot of COX-2 which was stripped with Restore^{TM} Western blot stripping buffer (Thermo Scientific) and reprobed for β-actin to correct for protein.

A.

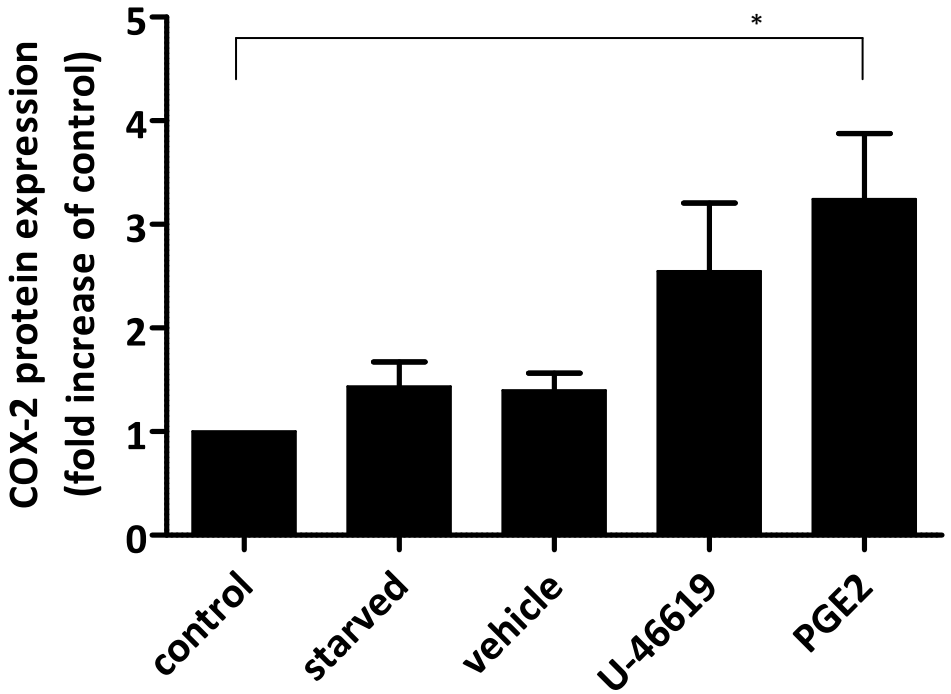
COX-2 protein expression
(fold increase of control)
5
4
3
2
1
0
*
control
starved
vehicle
U-46619
PGE2

B.

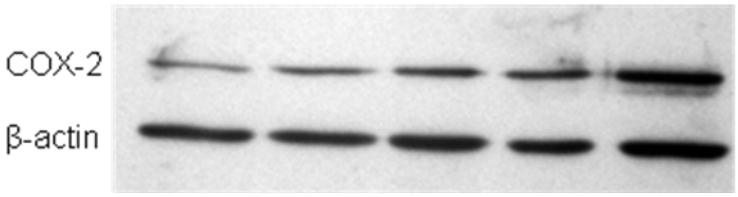
COX-2
β-actin

6.2. IN VIVO

6.2.1. Identification of candidate founders (I)

Of 15 pups born, one male candidate founder was identified (Fig. 6.9). This male was paired; its pups were genotyped and sacrificed for characterization.

6.2.2. NPHS1-2xHA-TPr^{mut} is not detectable by IF in founder (I)

Several different antibodies specific for the hemagglutinin epitope (Invitrogen; Clontech; Sigma-Aldrich) were used but fluorescence was not detected (Fig 6.10.)

6.2.3. Normal renal histology in founder (I)

A transgenic mouse was sacrificed and kidney tissue was stained with periodic acid-schiff as well as hematoxylin and eosin to determine any morphological abnormalities in the kidney potentially caused by NPHS1-2xHA-TPr^{mut} construct (Fig. 6.11). No abnormalities were noted.

6.2.4. Identification of candidate founders (II)

Of 18 pups born, no candidate founders could be identified with gel electrophoresis (Fig 6.12).

Figure 6.9. PCR products separated by agarose gel electrophoresis (I). Genomic DNA was extracted from 15 pups and added to a PCR reaction containing primers and REDExtract-N-Amp PCR ReadyMix. The fluorescent band at the leftmost lane indicates the presence of a candidate founder. The band on the right indicates the positive control (purified construct DNA used for microinjection). L = 100 bp marker (Invitrogen).


325 bp
+

Figure 6.10. Immunofluorescence in kidney of candidate founder offspring (I). 6 micron sections of kidney tissue are shown (A-B). Sections were examined with a fluorescent microscope (x200, Zeiss). (A) Transgenic offspring show no immunofluorescence for the HA-tag in glomeruli (arrows). (B) Wildtype control.

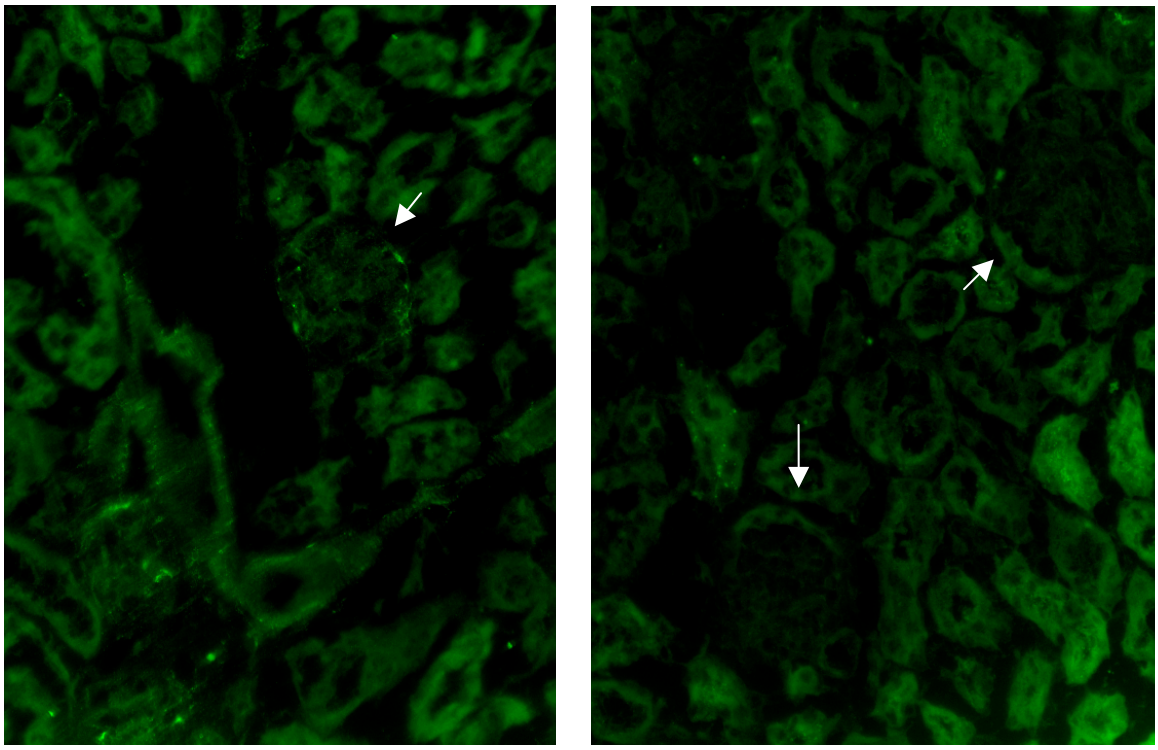

Figure 6.11. Renal histology (I). 6 micron sections of kidney tissue fixed in PFA are shown (A-B). Magnification x200 in (A-B) under light microscope (Zeiss) (A), periodic acid-Schiff (PAS) staining. (B) Hematoxylin and eosin staining. Glomerular tissue appears healthy (arrows).

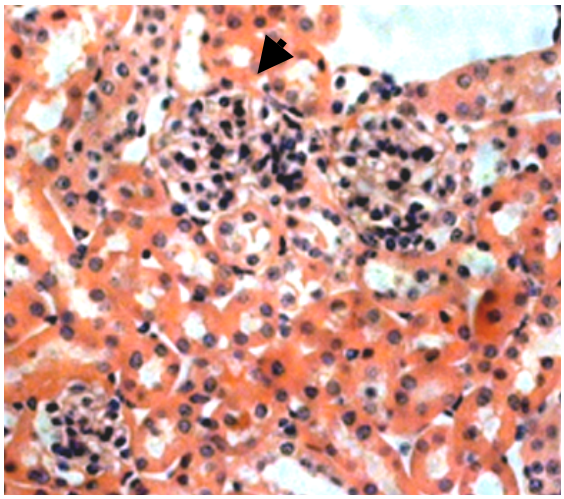

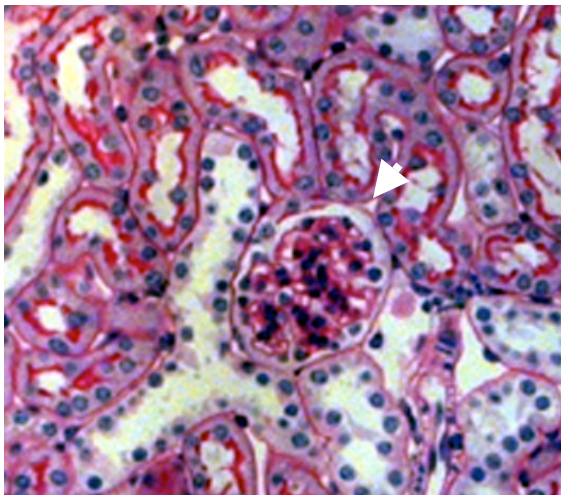

Figure 6.12. PCR products separated by agarose gel electrophoresis (II). Genomic DNA was extracted from 18 pups and added to a PCR reaction containing primers and REDExtract-N-Amp PCR ReadyMix. No candidate founders were detected.+ = positive control. L = 100 bp marker (Invitrogen).

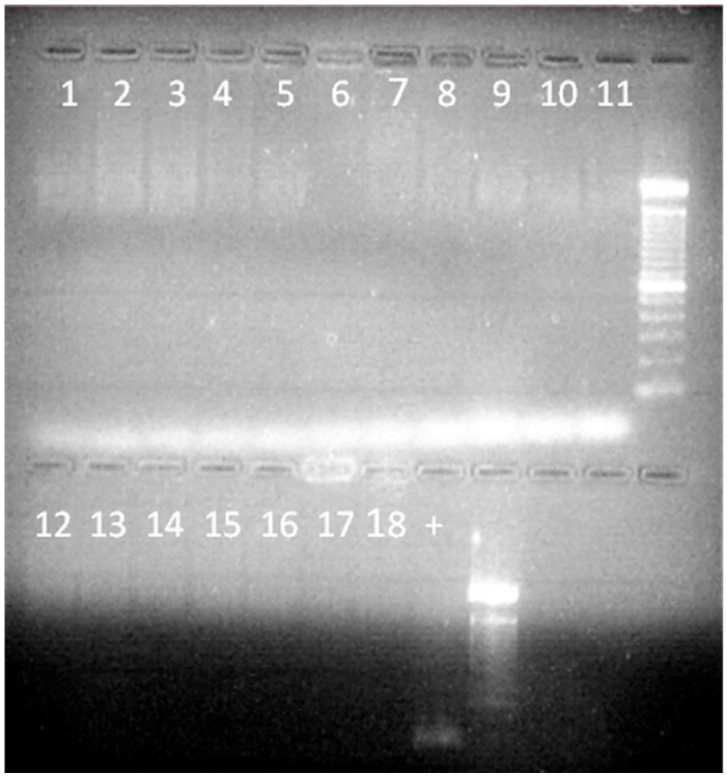
1 2 3 4 5 6 7 8 9 10 11
12 13 14 15 16 17 18 +

6.2.5. Identification of candidate founders (III)

Following the third series of DNA microinjections, all fertilized eggs had arrested at the late pronuclear stage and did not proceed to the 2-cell stage required for subsequent implantation into pseudopregnant CD-1 females for embryo development.

6.2.6. Identification of candidate founders (IV)

Of 31 pups born, two female and three male candidate founders were identified (Fig. 6.13). Following animal transfer to our isolation facility, three candidate founders died of unknown causes. Necropsy by the facility veterinarian was unremarkable. One viable male (4453) has produced 4 litters and a total of 6 transgenic offspring. The deceased male, 4458, went on to breed 1 litter and a total of 8 transgenic mice before dying. Transgenic offspring were sacrificed at 4 weeks of age for characterization using immunofluorescence. An antibody specific for the hemagglutinin epitope (Santa Cruz Biotech) was used but could not detect protein.

6.2.7. Estimates of transgene expression among founders (IV)

To obtain a quantitative estimate of the transgene expression, PCR amplification of genomic DNA was performed with primers designed to amplify a segment between the TPr gene and its 3'end HA-tag (corrected against GAPDH). Candidate founder 4458 appears to have the highest levels while 4453 is the lowest (Fig. 6.14) relative to control wildtype.

Figure 6.13. PCR products separated by agarose gel electrophoresis (IV). Genomic DNA was extracted from 31 pups and added to a PCR reaction containing primers and REDExtract-N-Amp PCR ReadyMix. The fluorescent bands indicate the presence of candidate founders. Ladder:100 bp marker (Invitrogen).

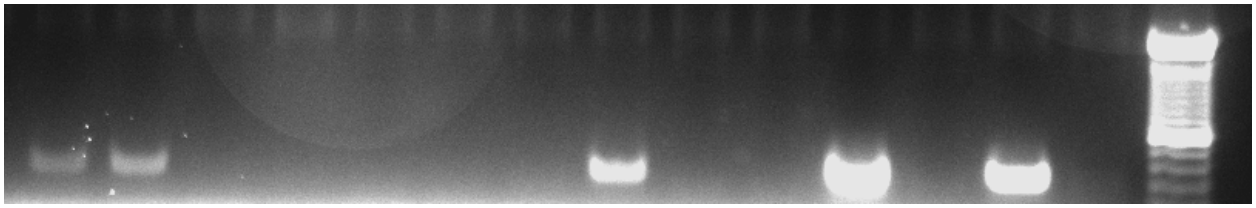

4446 4447 4453 4456 4458

Figure 6.14 . Estimate of transgene expression in genomic DNA of candidate founders. Values are expressed as fold increase of control of NPHS1-2xHA-TPr^{mut}/GAPDH ratios. qRT-PCR amplification of genomic DNA was performed using primers specific to the TPr-3' end HA-tag segment (normalized to GAPDH). Candidate founder 4458 expressed a 4.6-fold increase compared to control. Candidate founder 4453 expressed an almost 2-fold increase compared to control.

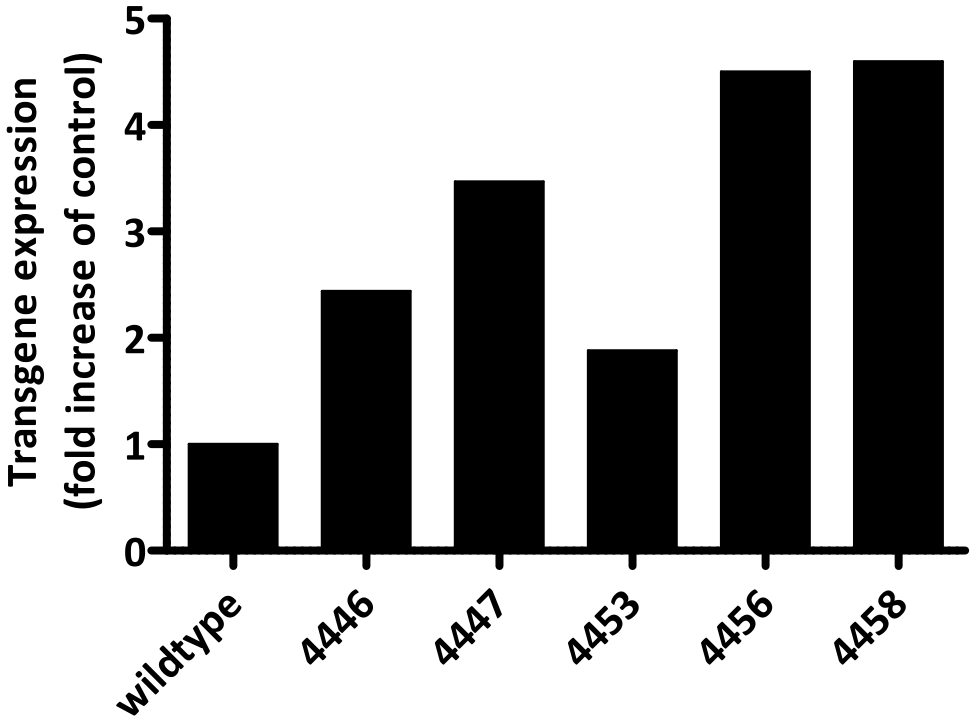
Transgene expression
(fold increase of control)
0
1
2
3
4
5
wildtype
4446
4447
4453
4456
4458

6.2.8. Normoalbuminuric founders (IV)

To determine whether the transgene conferred any damage to glomerular filtration function, spot urinalysis was performed on wildtype and founder lines. Transgenic mice from both lines albumin-to-creatinine (ACR) ratios are not significantly different from wildtype (Fig. 6.15).

6.2.9. Normal renal histology in founders (IV)

Both founders showed normal glomerular shape and appearance compared to wildtype following periodic acid-schiff and hematoxylin and eosin staining (Fig. 6.16).

6.2.10 Enhanced transgene mRNA expression observed in founder lines (IV)

To assess for the presence of the transgene, qRT-PCR was performed on RNA previously extracted from whole kidney tissue with primers specific to the TPr-3' end HA-tag segment. Both founder lines have enhanced mRNA levels compared to wildtype (approximately 3-fold) (Fig. 6.17).

6.2.11 . NPHS1-2xHA-TPr^{mut} is not detectable by Immunofluorescence in founder (IV)

IF was performed as with previous founder, with antibodies specific for the hemagglutinin epitope (Santa Cruz). Expression of the transgene cannot yet be reliably ascertained since this antibody showed non-specific cross-reactivity to some unknown antigen specifically in the glomerulus, as evidenced by its expression in the glomeruli of both transgenic and wildtype mice alike (Fig 6.18)

Figure 6.15. Urinalysis of founder lines. Values are expressed as ratios of albumin (µg) to creatinine (mg). ACR ratios are not significantly different between founders 1 and 2 and wildtype groups.

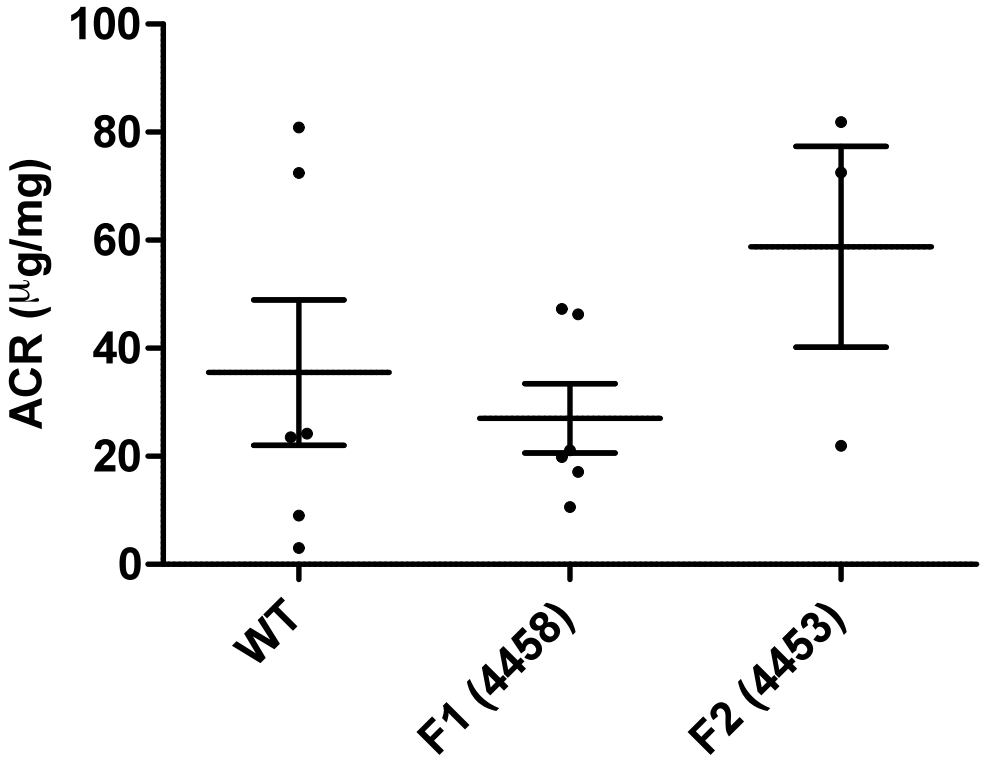
100
80
60
40
20
0
ACR (μg/mg)
WT
F1 (4458)
F2 (4453)

Figure 6.16. Renal histology (IV). 6 micron sections of kidney tissue fixed in PFA are shown. Magnification x200 under light microscope (Zeiss). Top panel: periodic acid-Schiff staining . Bottom panel: hematoxylin and eosin staining . Both founders have normal glomerular shape and appearance as in wildtype (arrows).

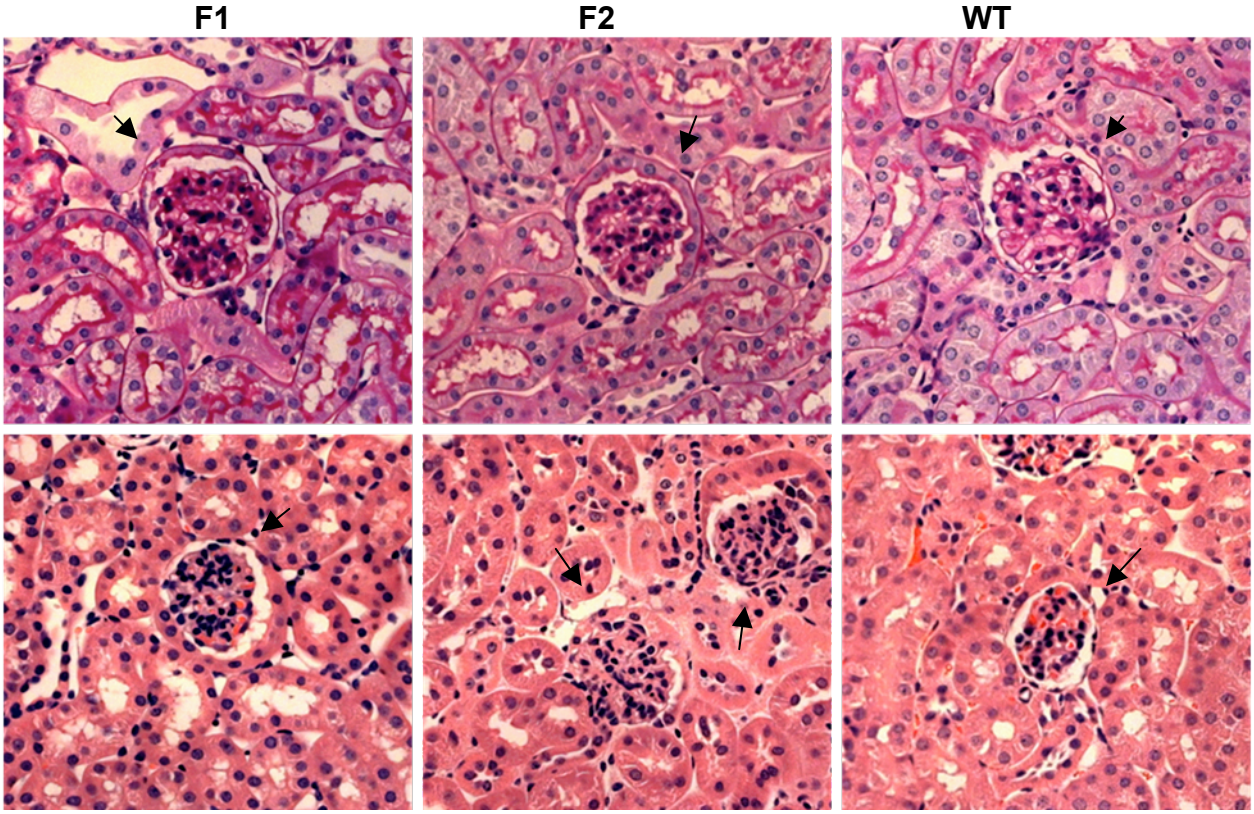
F1
F2
WT

Figure 6.17. Transgene mRNA expression. Values are expressed as ratios of concentration of NPHS1-2xHA-TPr^{mut} to GAPDH (ng/µl). Founders express enhanced mRNA levels compared to wildtype.

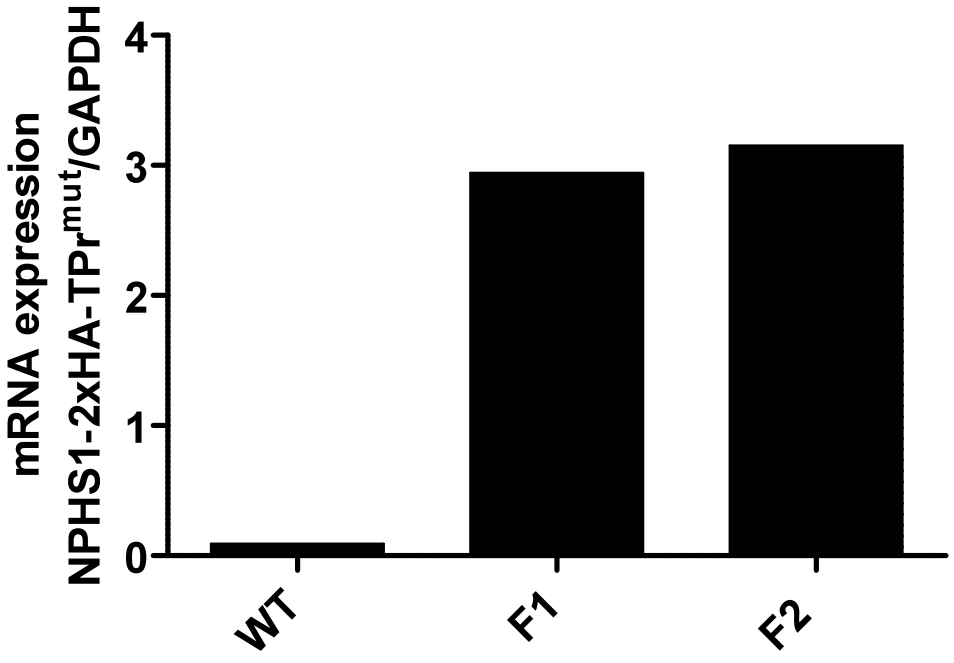
mRNA expression
NPHS1-2xHA-TPr^mut/GAPDH
4
3
2
1
0
WT
F1
F2

Figure 6.18. Immunofluorescence in kidney of candidate founder offspring (IV). 6 micron sections of kidney tissue are shown (A-C). Sections were examined with a fluorescent microscope (x200, Zeiss). Transgenic offspring show glomerular fluorescence of HA tag (arrows), however this also unexpectedly occurs in the wildtype, indicating false cross-reactivity of the antibody with some unknown antigen. Antibody also appears to bind to non-specifically to arterioles.

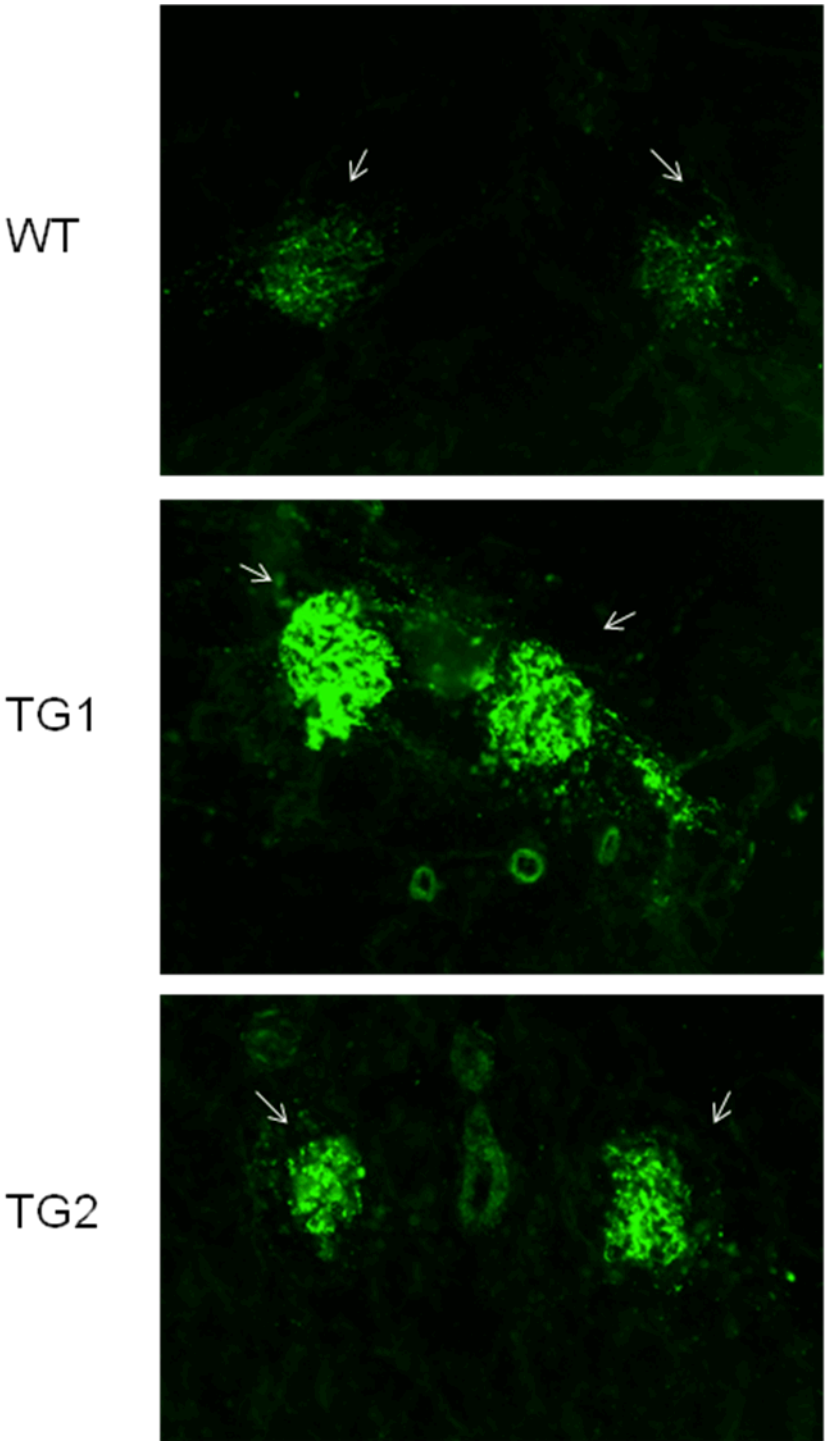
WT
TG1
TG2

7. DISCUSSION

7.1. IN VITRO STUDIES

The maladaptive role for TPr activity is observed across a spectrum of kidney disease models in animals, suggesting that this signaling pathway contributes to renal injury. Furthermore, the renoprotective effects of pharmacological TPr blockade has been shown in uninephrectomized obese Zucker rats[36], Streptozotocin (STZ) -induced type I diabetic rats[39,40], STZ-induced diabetic apolipoprotein $E^{-/-}$ mice[30], as well as rats with angiotensin-II induced nephropathy[41], progressive kidney disease from subtotal renal ablation[42] and murine lupus nephritis[39,43].

Studies examining deletion of TPr have shown its role in preserving systemic hemodynamics[44] as well as renal vasoconstriction during endotoxemic shock[45] and is implicated in hepatic microcirculatory dysfunction[46].

Aside from its role in maintaining renal and system hemodynamics , the TPr is also able to elicit specific and local effects to the glomerulus. Radeke and colleagues showed that mesangiolysis was associated with enhanced TxB_2 secretion from cultured mesangial cells[47]. Furthermore, Sebekova and colleagues showed that TPr is linked to mesangiolysis in uninephrectomized obese Zucker rats[36]. Since podocytes, mesangial and parietal epithelial cells exist in close proximity and express TPr, TxA_2 secretion could activate this signaling pathway in either an autocrine or paracrine manner in the glomerulus. However, the mechanisms of TPr activity in glomerular injury are still unclear.

Shedding light on this, our apoptosis studies serve as evidence of one of the mechanisms by which TPr activity is injurious to podocytes. Following 24-hour exposure to pharmacological agonism with U-46619, podocytes are significantly more vulnerable to cell death. Hoescht and Annexin V-FITC labeling revealed moderate increases in apoptosis, while TUNEL staining showed much greater increases. One reason for this discrepancy may be the method of cell counting, where the latter method employed quantified apoptosis by number of apoptotic cells divided by total number of cells averaged over five magnification fields; the number of cells quantified were much lower than with Hoescht (~300) and Annexin V (~1000). Despite this inconsistency, the pro-apoptotic effect of TP signaling is significant in the majority of methods used.

In support of our findings, Cheng and colleagues recently showed that administration of the same TP agonist, U-46619, significantly enhanced death in COX-2 overexpressing cultured podocytes subjected to puromycin aminonucleoside (PAN)-induced injury compared to podocytes not administered the agonist[19]. A commonly used experimental model of minimal change kidney disease is the injection of puromycin aminocleoside (PAN) that causes foot process effacement and proteinuria.

In the podocyte, numerous G-protein coupled receptors (GPCRs) have been linked to glomerular disease, including TPr, E-series prostaglandins (EP_1 receptor) and angiotensin II (AT_1 receptor). Although the signaling pathways that are activated by these GPCRs are diverse, common to all of these receptor systems is Gq signaling cascade activation. TPr employs the Gqα subunit protein that leads to

signaling via intracellular mobilization of Ca2+. Spurney and colleagues showed that overexpression of a constitutively active Gq α subunit induced podocyte death *in vitro*. TPr-mediated apoptosis may involve Gq-dependent activation of Protein Kinase C-zeta, which has been shown to modulate Akt activity, a protein involved in promoting cell viability[48,49].

Further studies examining whether the mechanism of TPr-mediated apoptosis occurs in a Gq-dependent fashion will be helpful in elucidating whether TPr can also initiate this potentially injurious signaling pathways in podocytes.

In vitro, upregulation of the Gq cascade induces COX-2 expression and is associated with podocyte death[50]. COX-2 overexpression has been shown to induce podocyte injury in a TPr-mediated fashion[51]. *In vivo*, TPr deletion in COX-2 overexpressing mice prevents adriamycin-induced injury, attenuates albuminuria as well as foot process effacement suggesting a distinct role for TPr-mediated glomerular injury induced by COX-2[52]. Our *in vitro* investigation of TPr activation and COX-2 expression suggests the presence of such a positive feedback relationship, however, additional experiments will be required to confirm the significance of this trend.

Another major suspect in glomerular injury is reactive oxygen species (ROS) generation. ROS are chemically active molecules containing oxygen; their enhanced production is induced by cellular stress. ROS are able to act as signaling molecules to alter cellular metabolism and mediate inflammatory responses. Cellular antioxidants such as manganese superoxide dismutase (MnSOD) and glutathione peroxidase (GTX) manage ROS production. ROS include the free radicals

superoxide (O_2•), hydroxyl (OH•), and non-radical species hydrogen peroxide (H_2O_2); their effects vary based on cellular localization and the balance between ROS and antioxidant activity. Cellular sources of ROS include mitochondria, NAD(P)H oxidases, cytochrome P450-based enzymes, xanthine oxidase and nitric oxide synthases[53,54].

Oxidative stress is a major contributor to the progression of diabetic complications[55]. Inhibition of NAD(P)H activity by apocynin is renoprotective in a mouse model of type II diabetes implicating ROS in DKD-associated glomerular injury[10]. Vega-Warner and colleagues showed that PAN treatment perturbs the balance of ROS and antioxidant enzyme activity defense, causing increased oxidant stress and injury[56]. NAD(P)H is the major source of superoxide in human podocytes[57]. Furthermore, ROS has been implicated in altering podocyte gene expression and modulate GPCR function and expression.

Cohen's group demonstrated a strong case for the role of oxidative stress in glomerular injury; they showed the potent antioxidant effects of TPr blockade in a mouse model of type II diabetes. Several markers of oxidant stress such as nitrotyrosine deposition, urinary levels of 8-isoprostane, 12-LOX, protein expression NAD(P)H oxidase subunit $p47^{phox}$,and inducible nitric oxide synthase (iNOS) were diminished, while a significant increase in the activity of the antioxidative enzyme, MnSOD was observed. They postulate that blockade of TPr interrupts a positive feedback loop in which activation of TPr stimulates the expression of NAD(P)H oxidase, 12-lipoxygenase, and iNOS which in turn produce oxidants that participate in tissue damage via lipid membrane peroxidation (pro-necrotic effects) and can

further produce 8-isoprostane and 12-HETE which can activate TPr in an autocrine fashion.

In support of this mechanism, Wilson and colleagues showed that ROS derived from NAD(P)H oxidases signal to drive TPr upregulation in a positive feedback loop fashion. TPr expression was augmented in TPα-transfected human embryonic kidney 293 cells treated with a TxA_2 analog, an effect which was blunted with NAD(P)H oxidase inhibition[58] .

In our experiment, oxidative stress was measured using the dihydroethidium probe for superoxide radicals. A significant trend could not be detected in podocytes treated with U-46619 compared to controls. Examining other markers of superoxide production such as iNOS, nitrotyrosine deposition, $p47^{phox}$, 12-LOX (an NAD(P)H cofactor), and other NADPH oxidases present in podocytes (Nox2, Nox4,Nox5) will be useful. Likewise, other superoxide radical probes could be employed, such as dihydrodichlorofluorescein (DCF) or lucigenin.

In the interest of relating our *in vitro* work to an *in vivo* context, the effects of TP activation in podocytes were studied upon introducing high extracellular glucose and mechanical stretch as a mimic of *in vivo* conditions of hyperglycemia and increased glomerular capillary pressure, respectively.

Mechanical stretch induces COX-2 upregulation[17] while mechanical stretch in concert with high extracellular glucose significantly upregulates TPr mRNA expression (Fig 1.6). This data combined with our findings that TPr activation is proapoptotic in podocytes suggest that podocytes would be more vulnerable to cell death due to TP activation under conditions of high extracellular glucose and stretch.

However, our TUNEL data examining podocytes subjected to combinations of these conditions and a TPr antagonist does not support this notion. Treating podocytes with high glucose and stretch alone does not enhance apoptosis compared to controls. Furthermore, administration of the TPr antagonist BM-567 does not exhibit any apparent protective effect on viability as might be anticipated. Whether high glucose and stretch instead promote another major endpoint of podocyte injury, such as cellular detachment; this could be measured by quantifying and comparing the number of podocytes found detached and floating in culture medium compared to the remaining adherent podocytes.

Besides the endpoint of apoptosis, we were interested in determining whether TP activation was induced in response to high extracellular glucose and stretch, since these very same conditions induced TPr mRNA expression levels in podocytes, particularly since Spurney and colleagues showed that TPr mRNA expression is associated with TxB_2 production in cultured podocytes[51]. Although Melina Marin-Leblanc was able to show that TP mRNA expression was enhanced in response to high extracellular glucose and stretch, whether TxB2 production was also enhanced remained to be seen. Upon performing an assay for the TxA_2 metabolite, TxB_2, our data demonstrate a potential trend where high extracellular glucose and mechanical stretch induce secretion of TxA_2. As mentioned, other ligands in addition to TxA_2 may bind TPr, including 12-HETE and 8-isoprostane; measuring these metabolites may also paint a more complete picture of TPr activation within podocytes.

7.2. IN VIVO STUDIES

In vivo, we asked whether podocyte TPr activation mediates GFB damage in a model of DKD, and we tested this hypothesis by developing a podocyte-specific overexpression model using a desensitization-resistant TPr that would prolong TPr signaling on the membrane.

We have thus far been able to show *NPHS1-2xHA-TPr^{mut}* mRNA transcript expression in our transgenic mice with immunofluorescence data showing increased fluorescence in transgenic founder tissue sections visualized by hemagglutannin tag-specific secondary antibodies. Further studies will need to confirm protein functionality. It would be most insightful to examine evidence of functionality of the injurious positive feedback loop between TPr activation and COX-2. Measuring COX-2 expression following TPr stimulation of isolated glomeruli would corroborate the observations of Cheng and Spurney[50,51]. Indeed, several attempts were made to measure COX-2 expression, specifically, mRNA using qRT-PCR and protein by western blot. Unfortunately, there were challenges in extracting sufficient amounts of either for quantification. Glomeruli that are isolated from mice contain small amounts of RNA and protein to work with, and future studies may need to reconsider this experiment with more sensitive tools.

Other downstream targets in the Gq-coupled pathway which could be used to assess for transgene functionality include the second messenger inositol-1,4,5-trisphosphate (IP_3) and Ca^{2+}. Specifically, stimulation of receptors coupled to G_q proteins activates PLC. This leads to hydrolysis of phosphatidylinositol 4,5-

bisphosphate (PIP_2) and generation of diacylglycerol (DAG) and IP_3, resulting in activation of PKC that prompts Ca^{2+} release from intracellular stores[59].

To ensure podocyte-specificity, our transgenic mouse model took advantage of the *NPHS1* promoter. *NPHS1* is also expressed in the brain and pancreas[60], but it is unlikely that our transgene disrupted developmental processes since all founders were healthy. Because our model was not a conditional one, transgenic mice were conferred the mutant receptor from the embryonic stage through adulthood. Transgenic mice demonstrated normal renal structure and function despite this; the transgene will require an additional 'hit', (ie. induction of diabetes) in order to elicit a palpable effect on renal function.

The conditional overexpression model of disease is the most preferred model of use, since it can be tightly controlled temporally and may more accurately reflect the human features of disease. However, we anticipate that the results of this study will establish whether TP activation promotes DKD through direct effects in the podocyte.

Although currently available animal models of diabetes strive to reflect the clinical case, no one model is able to mirror human disease completely. This challenge is multifactorial; the onset, similarity and severity of pathophysiological symptoms is affected by the strain, age, diet and genetic background of the animal.

Commonly used models of type I diabetes are the non-obese diabetic (NOD), Akita and the STZ-treated mouse. The NOD mouse strain develops diabetes as a result of autoimmune destruction of β-cells in the pancreas. Although this form of

diabetes leads to albuminuria, mild mesangial expansion and GBM thickening[61], the time onset of diabetes is variable and occurs late in life; furthermore, this strain lacks an appropriate control cohort because of its complex, multigenic background.

The Akita spontaneous mutation in the insulin II gene confers mice with abnormal insulin production, resulting in diabetes[62]. Currently, this mutation only exists in the C56BL/6J strain of mouse that appears resistant to DKD as denoted by its failure to develop prominent histopathological signs or albuminuria.

Streptozotocin is an antibiotic that, following injection, degenerates the beta cells of the pancreas, resulting in hyperglycemia. Type I diabetes manifests due to the animal's reduced capacity for insulin secretion. Type I diabetes persists for the lifespan of the animal[63]. The administration of low-dose STZ administration circumvents the non-specific cytotoxicity encountered in high-dose treatment while still achieving hyperglycemia and the onset of diabetes by β-cell destruction. These mice however develop variable, strain-dependent levels of albuminuria and modest mesangial matrix expansion[64].

A widely used model of type II diabetes is the *db/db* mouse, which possesses a recessive mutation in the leptin receptor of the hypothalamus, leading to obesity and diabetes. Although this mutation confers relatively prominent DKD development, it does not necessarily reflect the nature of the majority of cases of type II diabetes[64]

We anticipate that following induction of DKD, our transgenic mice will be rendered more susceptible to renal injury compared to non-transgenic controls. Future studies will expand the founder lines and introduce a STZ-induced model of type II diabetes. The experimental model will consist of four groups: (i) non-

transgenic with vehicle, (ii) non-transgenic with low-dose STZ (50 mg/kg/day, intraperitoneally for 5 days), (iii) transgenic with vehicle, (iv) transgenic with low-dose STZ. These groups will be followed for 16 weeks and assessed bi-weekly for blood pressure, albumin-to-creatinine ratios and blood glucose levels. Urine collection over 24 hours will be performed at the outset, mid-point and termination of the study. Mice will then be sacrificed and kidneys will be evaluated for renal and podocyte injury. Compromised podocyte integrity will be quantified as foot process effacement and apoptosis. We anticipate that STZ-treated transgenic mice will manifest significantly worse renal injury compared to wildtype as a result of enhanced TPr activation.

7.3. FUTURE DIRECTIONS

As mentioned, one major endpoint of podocyte injury and subsequent GFB destruction is detachment of podocytes from the GBM. Erin Stitt-Cavanaugh in our laboratory has extensively explored the role of the EP_4 prostanoid receptor in podocyte dysfunction. She has shown that mechanical stretch of podocytes overexpressing EP_4 detach from the extracellular matrix and lose stress fibers[65]. Furthermore, podocyte-specific EP_4 overexpression renders mice significantly more albuminuric with lower survival rates following removal of 5/6 of kidney mass. Conversely, depletion of the EP_4 receptor ameliorated these outcomes[65].

Proteins involved in actin cytoskeletal remodeling are Rho family proteins composed of members small GTPase RhoA, Cdc42 and Rac1. Their functions

include adhesion and stress fiber formation; they can promote cell attachment but also disrupt these structures to allow for dynamic rearrangements that permit shape change[66]. The capacity for the podocyte to undergo dynamic cytoskeletal remodeling is central to its ability to adapt to changing glomerular capillary pressures while preserving filtration function.

A mechanism by which TPr activation could elicit glomerular injury might be via cytoskeletal dysfunction. GPCR signaling is known to regulate Rho function[67]. Gq signaling mediates PKC phosphorylation which has been shown to phosphorylate Rho exchange factors[68] as well as Gα12 and Gα13[69,70], units which interact directly with Rho exchange factor. Rho-associated protein kinase (ROCK) is a downstream effector protein of RhoA. Denniss and colleagues showed that in rat common carotid artery, TPr signaling and ROS induce RhoA/ROCK signaling and enhance contractile activity[71]. Based on these findings, a role for TPr activation in podocyte cytoskeletal dysfunction is implied. Future studies examining the relationship betweenTPr agonism, RhoA/ROCK signaling and detachment, as well as ROS production will be valuable.

Former summer student Laura McLeod in our laboratory recently isolated mRNA from cultured podocytes following U-46619 stimulation. cDNA microarray analysis will be used to profile gene expression and identify genes whose expression may have changed in response to TPr agonism, such as those implicated in apoptotic pathways (upregulation of PKC-zeta, upregulation of proapoptotic p38 mitogen-activated protein kinase, upregulation of apoptosis-signaling protein caspase 3, downregulation of survival factor Akt) and oxidative

stress pathways (upregulation of $p47^{phox}$, iNOS, 12-LOX, downregulation of MnSOD).

7.4. SUMMARY

The major findings of this project are that TPr activation in culture podocytes elicits pro-apoptotic effects. Therapies aimed at blocking TPr signaling specifically in the podocyte may therefore preserve the viability of these non-proliferative and specialized cells. Upon future completion of the *in vivo* component of this project, it is anticipated that our *NPHS1-2xHA-TPr*^{mut} mouse model of type I diabetes will provide evidence of worsened renal structure and function due to specific effects of TPr activation on the podocyte.

8. REFERENCES

1. Overgaard, A.J*., et al.* Quantitative iTRAQ-Based Proteomic Identification of Candidate Biomarkers for Diabetic Nephropathy in Plasma of Type 1 Diabetic Patients. *Clin Proteomics* **6**, 105-114 (2010).
2. Schrier, R. *Diseases of the Kidney & Urinary Tract: Clinicopathologic Foundations of Medicine.*, (Lippincott Williams & Wilkins., 2007).
3. Pavenstadt, H., Kriz, W. & Kretzler, M. Cell biology of the glomerular podocyte. *Physiol Rev* **83**, 253-307 (2003).
4. Jefferson, J.A., Shankland, S.J. & Pichler, R.H. Proteinuria in diabetic kidney disease: a mechanistic viewpoint. *Kidney Int* **74**, 22-36 (2008).
5. Meyer, T.W., Bennett, P.H. & Nelson, R.G. Podocyte number predicts long-term urinary albumin excretion in Pima Indians with Type II diabetes and microalbuminuria. *Diabetologia* **42**, 1341-1344 (1999).
6. Pagtalunan, M.E*., et al.* Podocyte loss and progressive glomerular injury in type II diabetes. *J Clin Invest* **99**, 342-348 (1997).
7. Steffes, M.W., Schmidt, D., McCrery, R. & Basgen, J.M. Glomerular cell number in normal subjects and in type 1 diabetic patients. *Kidney Int* **59**, 2104-2113 (2001).
8. Toyoda, M., Najafian, B., Kim, Y., Caramori, M.L. & Mauer, M. Podocyte detachment and reduced glomerular capillary endothelial fenestration in human type 1 diabetic nephropathy. *Diabetes* **56**, 2155-2160 (2007).
9. Li, J.J*., et al.* Podocyte biology in diabetic nephropathy. *Kidney Int Suppl*, S36-42 (2007).
10. Susztak, K., Raff, A.C., Schiffer, M. & Bottinger, E.P. Glucose-induced reactive oxygen species cause apoptosis of podocytes and podocyte depletion at the onset of diabetic nephropathy. *Diabetes* **55**, 225-233 (2006).
11. Kojima, K., Matsui, K. & Nagase, M. Protection of alpha(3) integrin-mediated podocyte shape by superoxide dismutase in the puromycin aminonucleoside nephrosis rat. *Am J Kidney Dis* **35**, 1175-1185 (2000).
12. Reddy, G.R., Kotlyarevska, K., Ransom, R.F. & Menon, R.K. The podocyte and diabetes mellitus: is the podocyte the key to the origins of diabetic nephropathy? *Curr Opin Nephrol Hypertens* **17**, 32-36 (2008).
13. Wolf, G., Chen, S. & Ziyadeh, F.N. From the periphery of the glomerular capillary wall toward the center of disease: podocyte injury comes of age in diabetic nephropathy. *Diabetes* **54**, 1626-1634 (2005).
14. Wang, J.L., Cheng, H.F., Zhang, M.Z., McKanna, J.A. & Harris, R.C. Selective increase of cyclooxygenase-2 expression in a model of renal ablation. *Am J Physiol* **275**, F613-622 (1998).
15. Sanchez, P.L., Salgado, L.M., Ferreri, N.R. & Escalante, B. Effect of cyclooxygenase-2 inhibition on renal function after renal ablation. *Hypertension* **34**, 848-853 (1999).
16. Horiba, N*., et al.* Subtotal nephrectomy stimulates cyclooxygenase 2 expression and prostacyclin synthesis in the rat remnant kidney. *Nephron* **91**, 134-141 (2002).
17. Martineau, L.C., McVeigh, L.I., Jasmin, B.J. & Kennedy, C.R. p38 MAP kinase mediates mechanically induced COX-2 and PG EP4 receptor expression in podocytes: implications for the actin cytoskeleton. *Am J Physiol Renal Physiol* **286**, F693-701 (2004).
18. Komers, R*., et al.* Immunohistochemical and functional correlations of renal cyclooxygenase-2 in experimental diabetes. *J Clin Invest* **107**, 889-898 (2001).

19. Cheng, H.F*., et al.* Cyclooxygenase-2 inhibitor blocks expression of mediators of renal injury in a model of diabetes and hypertension. *Kidney Int* **62**, 929-939 (2002).
20. Karalliedde, J. & Viberti, G. Microalbuminuria and cardiovascular risk. *Am J Hypertens* **17**, 986-993 (2004).
21. Basi, S. & Lewis, J.B. Microalbuminuria as a target to improve cardiovascular and renal outcomes. *Am J Kidney Dis* **47**, 927-946 (2006).
22. Hao, C.M. & Breyer, M.D. Physiological regulation of prostaglandins in the kidney. *Annu Rev Physiol* **70**, 357-377 (2008).
23. Dubois, R.N*., et al.* Cyclooxygenase in biology and disease. *FASEB J* **12**, 1063-1073 (1998).
24. Nakahata, N. Thromboxane A2: physiology/pathophysiology, cellular signal transduction and pharmacology. *Pharmacol Ther* **118**, 18-35 (2008).
25. Baylis, C. Effects of administered thromboxanes on the intact, normal rat kidney. *Ren Physiol* **10**, 110-121 (1987).
26. Scharschmidt, L.A., Lianos, E. & Dunn, M.J. Arachidonate metabolites and the control of glomerular function. *Fed Proc* **42**, 3058-3063 (1983).
27. Beckman, J.S. & Koppenol, W.H. Nitric oxide, superoxide, and peroxynitrite: the good, the bad, and ugly. *Am J Physiol* **271**, C1424-1437 (1996).
28. Antonipillai, I*., et al.* A 12-lipoxygenase product, 12-hydroxyeicosatetraenoic acid, is increased in diabetics with incipient and early renal disease. *J Clin Endocrinol Metab* **81**, 1940-1945 (1996).
29. Natarajan, R. & Reddy, M.A. HETEs/EETs in renal glomerular and epithelial cell functions. *Curr Opin Pharmacol* **3**, 198-203 (2003).
30. Xu, S*., et al.* The thromboxane receptor antagonist S18886 attenuates renal oxidant stress and proteinuria in diabetic apolipoprotein E-deficient mice. *Diabetes* **55**, 110-119 (2006).
31. Bresnahan, B.A., Le Breton, G.C. & Lianos, E.A. Localization of authentic thromboxane A2//prostaglandin H2 receptor in the rat kidney. *Kidney Int* **49**, 1207-1213 (1996).
32. Murray, R., Shipp, E. & FitzGerald, G.A. Prostaglandin endoperoxide/thromboxane A2 receptor desensitization. Cross-talk with adenylate cyclase in human platelets. *J Biol Chem* **265**, 21670-21675 (1990).
33. Houslay, M.D., Bojanic, D. & Wilson, A. Platelet activating factor and U44069 stimulate a GTPase activity in human platelets which is distinct from the guanine nucleotide regulatory proteins, Ns and Ni. *Biochem J* **234**, 737-740 (1986).
34. Yamamoto, K., Ebina, S., Nakanishi, H. & Nakahata, N. Thromboxane A2 receptor-mediated signal transduction in rabbit aortic smooth muscle cells. *Gen Pharmacol* **26**, 1489-1498 (1995).
35. Ally, A.I. & Horrobin, D.F. Thromboxane A2 in blood vessel walls and its physiological significance: relevance to thrombosis and hypertension. *Prostaglandins Med* **4**, 431-438 (1980).
36. Sebekova, K., Eifert, T., Klassen, A., Heidland, A. & Amann, K. Renal effects of S18886 (Terutroban), a TP receptor antagonist, in an experimental model of type 2 diabetes. *Diabetes* **56**, 968-974 (2007).
37. Constantini, F., et al. *Manipulating the mouse embryo: A laboratory manual*, (1986).
38. Takemoto, M*., et al.* A new method for large scale isolation of kidney glomeruli from mice. *Am J Pathol* **161**, 799-805 (2002).
39. Matsuo, Y*., et al.* Antiproteinuric effect of a thromboxane receptor antagonist, S-1452, on rat diabetic nephropathy and murine lupus nephritis. *Pharmacology* **50**, 1-8 (1995).

40. Uriu, K., Kaizu, K., Hashimoto, O., Komine, N. & Etoh, S. Acute and chronic effects of thromboxane A2 inhibition on the renal hemodynamics in streptozotocin-induced diabetic rats. *Kidney Int* **45**, 794-802 (1994).
41. Sebekova, K., Ramuscak, A., Boor, P., Heidland, A. & Amann, K. The selective TP receptor antagonist, S18886 (terutroban), attenuates renal damage in the double transgenic rat model of hypertension. *Am J Nephrol* **28**, 47-53 (2008).
42. Purkerson, M.L.*, et al.* Inhibition of thromboxane synthesis ameliorates the progressive kidney disease of rats with subtotal renal ablation. *Proc Natl Acad Sci U S A* **82**, 193-197 (1985).
43. Spurney, R.F.*, et al.* Thromboxane receptor blockade reduces renal injury in murine lupus nephritis. *Kidney Int* **41**, 973-982 (1992).
44. Thomas, D.W.*, et al.* Coagulation defects and altered hemodynamic responses in mice lacking receptors for thromboxane A2. *J Clin Invest* **102**, 1994-2001 (1998).
45. Boffa, J.J., Just, A., Coffman, T.M. & Arendshorst, W.J. Thromboxane receptor mediates renal vasoconstriction and contributes to acute renal failure in endotoxemic mice. *J Am Soc Nephrol* **15**, 2358-2365 (2004).
46. Katagiri, H.*, et al.* TNF-alpha induces thromboxane receptor signaling-dependent microcirculatory dysfunction in mouse liver. *Shock* **30**, 463-467 (2008).
47. Radeke, H.H., Kuster, S., Kaever, V. & Resch, K. Effects of cyclosporin and FK-506 on glomerular mesangial cells. Evidence for direct inhibition of thromboxane synthase by low cyclosporin concentrations. *Eur J Clin Pharmacol* **44 Suppl 1**, S11-16 (1993).
48. Shizukuda, Y. & Buttrick, P.M. Protein kinase C-zeta modulates thromboxane A(2)-mediated apoptosis in adult ventricular myocytes via Akt. *Am J Physiol Heart Circ Physiol* **282**, H320-327 (2002).
49. Garcia-Hoz, C.*, et al.* G alpha(q) acts as an adaptor protein in protein kinase C zeta (PKCzeta)-mediated ERK5 activation by G protein-coupled receptors (GPCR). *J Biol Chem* **285**, 13480-13489.
50. Wang, L., Flannery, P.J., Rosenberg, P.B., Fields, T.A. & Spurney, R.F. Gq-dependent signaling upregulates COX2 in glomerular podocytes. *J Am Soc Nephrol* **19**, 2108-2118 (2008).
51. Cheng, H.*, et al.* Distinct Roles for Basal and Induced COX-2 in Podocyte Injury. *J Am Soc Nephrol*, ASN.2009010039 (2009).
52. Cheng, H.*, et al.* Distinct roles for basal and induced COX-2 in podocyte injury. *J Am Soc Nephrol* **20**, 1953-1962 (2009).
53. Pongnitmitprasert. Atherosclerosis and NADPH oxidase. *Silpakorn U Science & Tech J* (2009).
54. Babior, B.M. NADPH oxidase. *Curr Opin Immunol* **16**, 42-47 (2004).
55. Evans, J.L., Goldfine, I.D., Maddux, B.A. & Grodsky, G.M. Oxidative stress and stress-activated signaling pathways: a unifying hypothesis of type 2 diabetes. *Endocr Rev* **23**, 599-622 (2002).
56. Vega-Warner, V., Ransom, R.F., Vincent, A.M., Brosius, F.C. & Smoyer, W.E. Induction of antioxidant enzymes in murine podocytes precedes injury by puromycin aminonucleoside. *Kidney Int* **66**, 1881-1889 (2004).
57. Greiber, S.*, et al.* NAD(P)H oxidase activity in cultured human podocytes: effects of adenosine triphosphate. *Kidney Int* **53**, 654-663 (1998).
58. Wilson, S.J.*, et al.* Activation-dependent stabilization of the human thromboxane receptor: role of reactive oxygen species. *J Lipid Res* **50**, 1047-1056 (2009).
59. Berridge, M.J. Inositol trisphosphate and calcium signalling. *Nature* **361**, 315-325 (1993).

60. Putaala, H., Soininen, R., Kilpelainen, P., Wartiovaara, J. & Tryggvason, K. The murine nephrin gene is specifically expressed in kidney, brain and pancreas: inactivation of the gene leads to massive proteinuria and neonatal death. *Hum Mol Genet* **10**, 1-8 (2001).
61. Sharma, K. & Ziyadeh, F.N. Renal hypertrophy is associated with upregulation of TGF-beta 1 gene expression in diabetic BB rat and NOD mouse. *Am J Physiol* **267**, F1094-1001 (1994).
62. Haseyama, T.*, et al.* Complications of IgA nephropathy in a non-insulin-dependent diabetes model, the Akita mouse. *Tohoku J Exp Med* **198**, 233-244 (2002).
63. Nugent, D.A., Smith, D.M. & Jones, H.B. A review of islet of Langerhans degeneration in rodent models of type 2 diabetes. *Toxicol Pathol* **36**, 529-551 (2008).
64. Breyer, M.D.*, et al.* Mouse models of diabetic nephropathy. *J Am Soc Nephrol* **16**, 27-45 (2005).
65. Stitt-Cavanagh, E.M.*, et al.* A Maladaptive Role for EP4 Receptors in Podocytes. *J Am Soc Nephrol*.
66. Karnoub, A. Rho Family GTPases and Cellular Transformation. in *Madame Curie Bioscience Database* (Landes Bioscience and Springer Science+Business Media, 2000).
67. Seasholtz, T.M., Majumdar, M. & Brown, J.H. Rho as a mediator of G protein-coupled receptor signaling. *Mol Pharmacol* **55**, 949-956 (1999).
68. Fleming, I.N., Elliott, C.M., Collard, J.G. & Exton, J.H. Lysophosphatidic acid induces threonine phosphorylation of Tiam1 in Swiss 3T3 fibroblasts via activation of protein kinase C. *J Biol Chem* **272**, 33105-33110 (1997).
69. Hart, M.J.*, et al.* Direct stimulation of the guanine nucleotide exchange activity of p115 RhoGEF by Galpha13. *Science* **280**, 2112-2114 (1998).
70. Offermanns, S., Hu, Y.H. & Simon, M.I. Galpha12 and galpha13 are phosphorylated during platelet activation. *J Biol Chem* **271**, 26044-26048 (1996).
71. Denniss, S.G., Jeffery, A.J. & Rush, J.W. RhoA-Rho kinase signaling mediates endothelium- and endoperoxide-dependent contractile activities characteristic of hypertensive vascular dysfunction. *Am J Physiol Heart Circ Physiol* **298**, H1391-1405.